Technische Universität Ilmenau

Faculty of Mechanical Engineering

Master Thesis

"Design and implementation of a test bench system for transfer of pressure sensor data"

To achieve the Degree:

Master of Science (M.Sc.)

in Mechatronics

Submitted by:	B.Sc. Antonio Esteban Fiestas Ugás
Date and Place of Birth:	14.08.1990 Trujillo (Peru)
Matrikel-Nr:	55180
Cod. PUCP:	20144163

Department (TU Ilmenau):	Biomechatronik
Advisor (TU Ilmenau):	M.Sc. Nelsón Enrique Bances Purizaca
Responsible Professor (TU Ilmenau):	Univ.-Prof. Dipl.-Ing. Dr. med. (habil.) Hartmut Witte
Responsible Professor (PUCP):	M.Sc. Francisco Fabián Cuéllar Córdova
Date and Place:	25.04.2016, Ilmenau

Declaration of autonomous work

Hereby, I declare that I have elaborated the present work without any nonspecified assistance. The people involved in the research, literature, as well as any other resource used in this thesis, has been completely specified throughout and at the end of the text.

In the course of the double degree program between TU-Ilmenau and Pontifical Catholic University of Peru, this thesis is presented in the examination offices of both universities. It was not presented in any other institution and was not published.

Ilmenau, den 25. 04. 2016 Antonio Esteban Fiestas Ugás

Kurzfassung

Heutzutage haben drahtlose Sensorvorrichtungen große Aufmerksamkeit in medizinischen Anwendungsbereichen erhalten; unter ihnen sind die implantierbaren Sensorvorrichtungen die wichtigsten wegen dem Beitrag, den sie zur medizinischen Versorgung und Untersuchungen leisten. Trotzdem müssen die implantierbaren Sensorvorrichtungen getestet werden bevor vorklinische oder "in-vivo-Studien" initiiert und Prüfstände verwendet werden um diese vorherigen Tests durchzuführen. Aus diesem Grund stellt die vorliegende Arbeit die Konzeption und Umsetzung eines Prüfstandes dar, der die Daten aus einer implantierbaren Sensorvorrichtung erwirbt, der entwickelt und verwendet wird, um den Druck in der Brusthöhle von Säugetieren zu erfassen. Der Prüfstand besteht aus einem verschlossenen Behälter mit zwei Anschlüsse um den Innendruck zu erhöhen und zu spüren und stellt gleichzeitig die Umgebung dar, in der der Sensor getestet wird, und einem drahtlosen Kommunikationssystem, das die Signale der Sensoren erfasst und verarbeitet. Dieses Kommunikationssystem besteht aus zwei Hauptmodulen, welche per Funk über das biomedizinische zugelassene Band von 433 MHz unter Verwendung eines implementierten Kommunikationsprotokoll miteinander kommunizieren. Schließlich sind die Kalibrierung und Tests auf einem pizoresistiven Drucksensor durchgeführt worden, um die Funktionalität des Systems zu beweisen und die Ergebnisse der Experimente werden dargestellt.

37 Abbildugen
8 Tabellen
47 Seiten

Abstract

Nowadays, wireless sensor devices have received wide attention across medical application areas; among them, implantable sensing devices are between the most important because of the contribution they make to healthcare and investigations. Nevertheless, the implantable sensing devices must be tested before pre-clinical or in-vivo studies are initiated and test benches are used to perform this previous tests. For this reason, this thesis presents the design and implementation of a test bench to acquire the data from an implantable sensing device that is being developed and will be used to sense the pressure within the thoracic cavity of mammals. The test bench consists on: a sealed container with two connections to increase and sense the internal pressure and is the environment where the sensor will be tested, and a wireless communication system that will acquire and process the sensor's signal and is consisted of two principal modules that will communicate between them via radio frequency at the biomedical admitted band of 433 MHz using an implemented communication protocol. Finally, the calibration and tests on a pizoresistive pressure sensor have been performed to prove the functionality of the system and the experiments results are presented.

37 Figures
8 Tables
47 Pages

Acknowledgment

I would like to express my gratitude to Prof. Hartmut Witte for his recommendations and support during the thesis project development.

In addition, I would like to thank Enrique Bances for giving me the thesis topic and, for his help, guidance, support and patience during the development and documentation of the thesis.

I would also like to express my gratitude to Prof. Francisco Cuellar, for his support as thesis supervisor.

Además, quisiera agradecer a mis padres Jesús y Delia, y mis hermanos Alan, Jackeline y David por todo el apoyo que me han brindado durante mi vida.

Finally, I would like to thank my friends, who always supported and motivated me.

Antonio Fiestas
Ilmenau, 25.04.2016

Abbreviations and Symbols

μC	Microcontroller
+OUT	Sensor bridge positve output
-OUT	Sensor bridge negative output
A	Linear regression's calculated slope
$A2D\_offset$	SSC's zero offset
A_{cal}	Calibration's slope
ADC	Analaog to Digital Converter
B	Linear regression's calculated y-axis intercept
B_{cal}	Calibration's y-axis intercept
CLK	SPI's Clock
CRC	Cyclic Redundance Check
GAIN	SSC's Gain
GUI	Graphic User Interface
I/O	Input/Output
I^2C	Inter Integrated Cirquit
IPSD	Implantable Pressure Sensig Device
ISD	Implantable Sensing Device
K_{cal}	Calibration's slope caluculated after the linear regression
MISO	SPI's Master Input Slave Output
MOSI	SPI's Master Output Slave Input
P	Sensed Pressure
RF	Radio Frequency
Rx	Reception
SOA	Sensor's Overall Accuracy
SoC	System on Chip
SPI	Serial Peripheral Interface
SS	SPI's Slave Select
SSC	Sensor's Signal Conditioner
Tx	Transmission
UART	Universal Asynchronous Receiver Transmitter

USART	Universal Synchronous Asynchronous Receiver Transmitter
V_{in}	System Supply Voltage
V_{out}	Voltage drop in between the sensor output terminals
X	Manometer's read
Y	Sensor's read before calibration
Y_0	Sensor's read at 0 mmHg
Y_{cal}	Calibration's y-axis intercept caluculated after the linear regression
Y_f	Sensor's calibrated read
Y_z	Sensor's read with zero correction
Z	Digital Value

Contents

List of Figures

List of Tables

1 Introduction

A test bench is an environment where a product under development is tested with the aid of software and hardware tools. This environment helps to optimize the product design and allows to test the implemented technology. Furthermore, test benches facilitate the design freezing in the development of medical devices before in-vivo studies are initiated.

The group of biomechatronic of the TU Ilmenau are developing an implantable sensing device to test the pressure within the thoracic cavity of mammals. This device allows to measure the pressure variation inside the chest during the locomotion of the animal. Hence, the design and implementation of a test bench is required to validate the device's design and evaluate the pressure sensor used.

The present thesis presents the design and implementation of a wireless communication system for pressure sensors data. This system allows the transmission and reception of the sensor data. In addition, this work reports the calibration and tests of the sensor in the implemented test bench.

Finally, the wireless communication protocol of the device is tested, as well as the graphic unit interface implemented to monitor the sensor data in real time.

The thesis starts with a brief introduction to test benches and the work aims. The Chapter 2 presents a short overview of the chest wall pressure curve modelling and, the current state of implantable sensing devices and a short review of test benches for pressure sensors.

In the Chapter 3 and 4, the design of the wireless communication system and the communication protocol implemented are described.

In Chapter 5, the implementation of a test bench for a piezoresistive pressure sensor

is described.

The Chapters 6 presents the results of the sensor's calibration and test made on the sensor.

Finally, general conclusions of the work are given in Chapter 7.

2 State of Art

2.1 Implantable Sensing Devices

Wireless sensor devices have received wide attention across medical application areas. In addition, for wireless data acquisition is convenient to make these devices small and with low power consumption [PLC05].

Implantable sensing devices (ISD) are a modern medical care prevalent part and have extended the ability to diagnose and treat diseases, making great contributions to health and quality of life [KMJD14].

ISD must have minimal size and weight, and low power, like the typical wireless sensor, for long term performance and the patient's safety [MJJ11]; in addition, ISD must have good reliability, high biocompatibility, minimal toxicity and, high data rate and data latency. Furthermore, the device's wireless communication should be performed in the Medical Implants Communication Services band of 402–405 MHz [BJ12] with a power level limited to 25 μW of Effective Radiated Power [YK07].

In addition, the ISD can be devided in two groups. On one hand there are battery driven systems, e.g., tip catheter based ones with wireless data transmission [BHK$^+$96]; nevertheless, the principal disadvantage of this systems is that with an increased complexity the battery lifetime decreases drastically [FCMIP91]. On the other hand, there are systems without an internal power source, e.g., the pressure monitoring systems developed by Schlierf and others [SHR$^+$07]; nevertheless, the transmission distance of this systems is limited [RPC$^+$00].

2.1.1 Implantable Pressure Sensing Devices

Nowadays, different types of implantable pressure sensing devices (IPSD) have been developed for medical applications. This implants were designed to sense pressure inside the skull, bladder, urinary tracks, etc.

Between the already designed IPSDs, there are some major differences in their design, some of the differences are listed as follows:

- In some designs the sensor is separated with the implant electronics and both parts are connected using a catheter; while, others have the sensor and electronics integrated in a single component.
- Some of the devices have a battery integrated in the implant to power the electronics and there are some powered by telemetry.
- The pressure transducer used in this devices are either a piezoresistive or a capacitive pressure sensor [KTW+08].

Despite of the difference in the implants design, the devices electronics used to acquire and transmit the sensor's signal are similar in the structure. To perform this, the electronic systems are consisted basically in a signal conditioner and a radio frequency transmitter, using a microcontroller as an intermediary between them. Moreover, the transmitted signal are received and displayed in an external station that can be a PC or a personal digital assistant [LJD+07].

In-vitro tests for IPSDs

The Figure 2.1 shows the schematic diagram of the test bench used to make in-vitro tests on an implantable pressure sensing device. This test benches consists on a pressure chamber where the sensor is introduced. The internal pressure on the chamber vary by introducing air inside it. Then, the pressure values given by the device are compared with an external manometer. Some of the studied IPSDs, e.g. [LJD+07], [KTW+08], have been tested using a similar technique to calibrate the sensor.

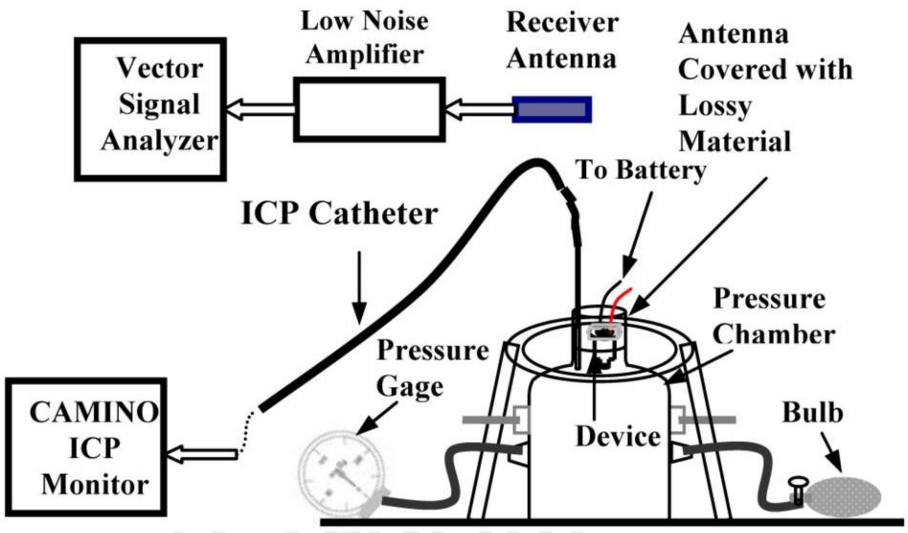

Figure 2.1: Schematic of the setup based on sphygmomanometer technique for monitoring air pressure. [KTW+08]

2.2 Respiratory System Mechanics and Chest Wall Pressure

The dynamic model that describes the relationship between the pressure variation at the airway opening during breathing (P_{AO}) and the lung volume (V) is expressed in Equation 2.1. The model assumes one degree of freedom, meaning that the expansion is isotropic [Har05].

$$P_{AO} = \frac{V}{C} + \dot{V}R + \ddot{V}I - P_{mus} \tag{2.1}$$

In the Equation 2.1 P_{mus} is the pressure generated by the respiratory muscles, C is respiratory system compliance, $\dot{V}$ is gas flow, R is airway resistance, $\ddot{V}$ is convective gas acceleration, and I is impedance.

What is evident from the model is that during an static analysis, the resistive and impedance effects on pressure are eliminated, and only the compliance is assessed. Furthermore, the respiratory muscle contribution to pressure is evident [Har05].

A static P-V curve can be obtained, if the analysis is done correctly and under the

correct conditions that allows to eliminate the effects of respiratory muscles on the pressure. Nevertheless, the system never reaches truly static conditions; so, the curve obtained is a quasi-static P-V curve which is used to describe the mechanical behaviour of the lungs and chest wall during inflation and deflation.

Another thing to consider during a static analysis is that the pressure on the respiratory system equals to the pressure at the airway opening and the sum of the chest wall (abdomen and ribs) and the lungs pressure; as shown in Equation 2.2 [CH05].

$$P_{AO} = P_{RS} = P_W + P_L \tag{2.2}$$

The Figure 2.2, shows the response the respiratory system, chest wall and lungs pressure during breathing. Furthermore, the figure shows the range on which the pressure vary for a healthy person.

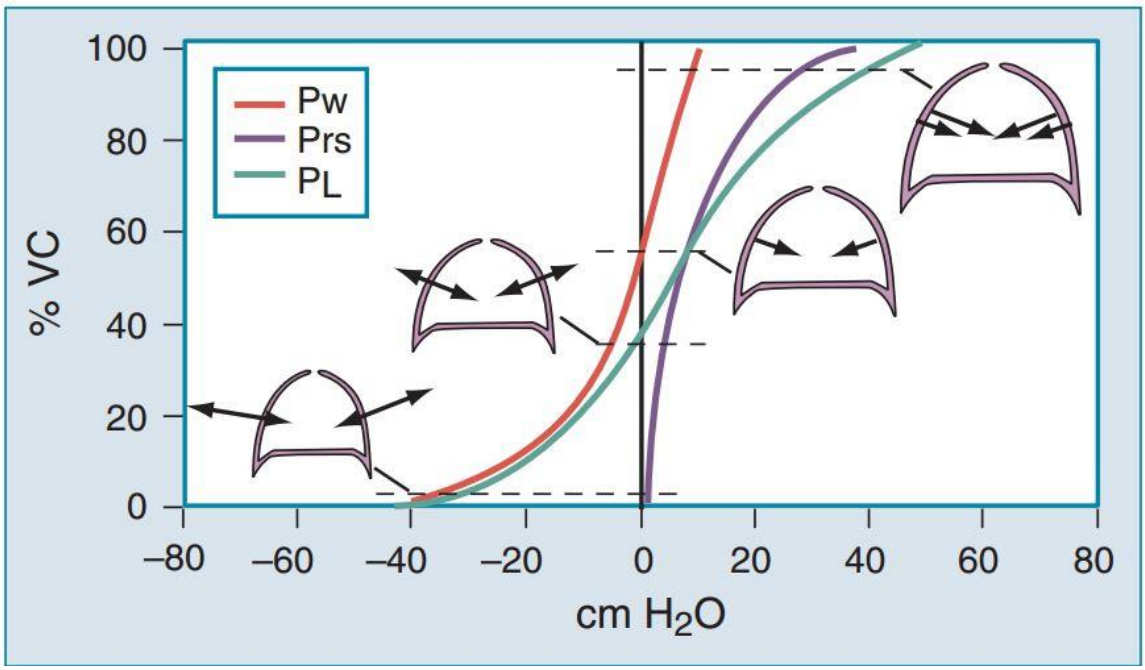

Figure 2.2: The normal sigmoid pressure-volume curve in an upright, awake, and relaxed subject. The pressure-volume curve of the respiratory system (PRS) is the sum of the pressures generated by the chest wall (PW) and lungs (PL).[AH86]

2.3 Wireless Radio Frequency Communication Systems

A wireless radio frequency system is composed by active and passive devices connected to perform a useful function. An example of this system is shown in 2.3.

The transmitter input is a digital bit stream, the digital data is modulated to an analog baseband signal (ABS). Then, the ABS is mixed with a radio carrier signal (RC) given by a local oscillator, which normally has a higher frequency, to produce a modulated carrier. Finally, the modulated carrier is then amplified and transmitted by an antenna using the established communication channel.

When the signal arrives at the receiver, is amplified by a low noise amplifier. Then, the amplified signal is demodulated to obtain the ABS. Finally, the ABS is decoded to obtain the original digital data. [Cha04]

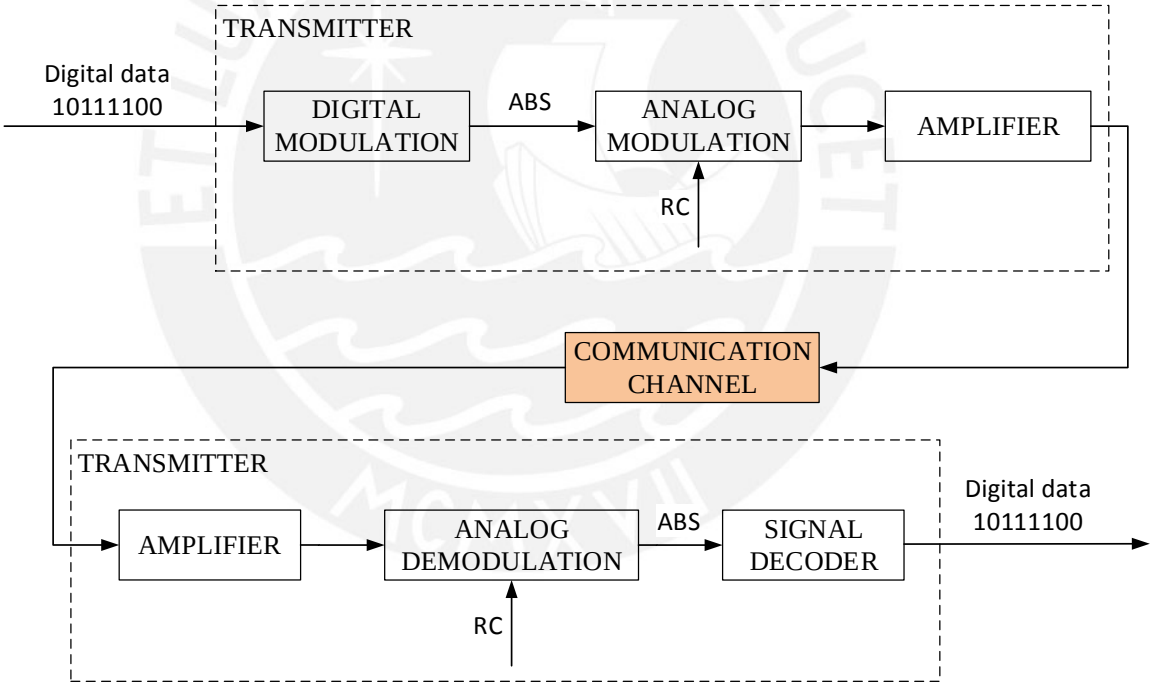

Figure 2.3: Radio Frequency Communication Block Diagram

3 Wireless Communication System

3.1 Design Scope

The wireless communication system is composed by two modules, one transmitter and one receiver. The main function is to transmit the pressure sensor signal wirelessly from the sensed point the a PC where the transmitted data can be shown and post processed.

The transmitter module consists by the follow structure: a sensor signal conditioner (SSC), and a system on chip (SoC) that integrates the microcontroller and radio frequency transceiver in the same chip. The SSC will amplify and digitalize the sensor analog signal and transmit the digital data to the microcontroller. The main function of the SoC's microcontroller is to manage the information between the SSC and the transceiver as a transmitter mode. As a receiver mode, the microcontroller manages the information received and set the communication with the PC, trough a graphic user interface (GUI). The transmitter module designed and implemented in this research, considers many practical characteristic as for example: it is transportable and power efficient because its principal power supply will be a battery; the module has output pins for signal evaluation and a port to connect another sensor, and allows serial communication with the PC in order to perform different tests and detect failures.

On the other hand, the receiver module, as we mention before, includes the SoC in receiver mode and a serial interface module, which allows the communication with the PC. The information given to the PC will be displayed through a graphic unit interface (GUI).

Finally, it is important to remark that in spite of the wireless communication for implantable devices should be in the range of 402-405 MHz, according to the international

norm for implantable devices [CMI13], the communication will be done by using the 433 Mhz band for medical devices [CMI13].

3.2 Block Diagram

The block diagram for the transmitter module and the receiver module are shown in the Figure 3.1 and Figure 3.2 respectively. The characteristics of each component and the selection criteria are shown in the next sections.

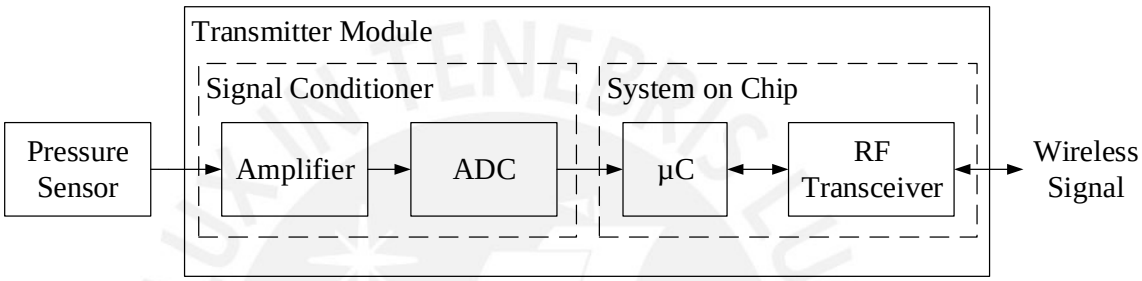

Figure 3.1: Transmitter module block diagram

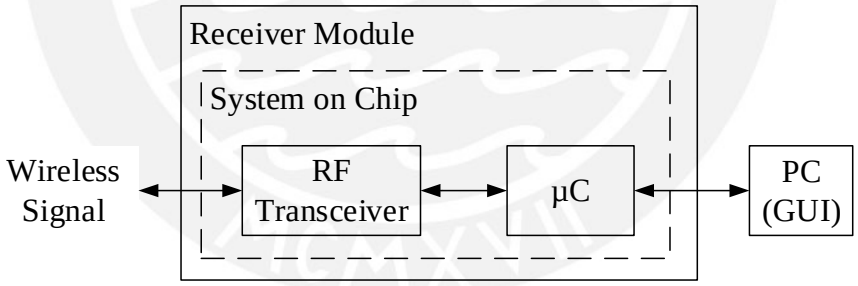

Figure 3.2: Receiver module block diagram

3.2.1 Transmitter Module

Pressure Sensor

As it was explained before the system will be used to sense internal chest wall pressure which range goes from $-40\ cmH_2O$ to $40\ cmH_2O$ [CH05][Har05] or $\pm 29.42\ mmHg$; hence, the sensor should work between this pressure ranges. Furthermore, the sensor's size and high reliability are two important features in an implantable device.

The table 3.1, shows some pressure sensors with similar characteristics in the market. From the list, the NPC100 is selected because it can work in the needed pressure range, has a small size and is available.

The NPC100 integrates a high-performance, piezoresistive sensor with a temperature compensation circuitry and gel protection in a small, low-cost package. Furthermore, the sensor sensitivity is maintained to $\pm 1\%$ and linearity is better than 1% in the physiological operating pressure range [Gen11].

In the figure 3.3 (left) displays the sensor aspect and (right) the sensor schematic diagram. The schematic diagram shows that a Wheatstone Bridge has already been integrated; where, +OUT and -OUT are the sensor's signal outputs, and +IN and -IN are the sensor's power input. Moreover, the sensor specifications are in the Appendix A.

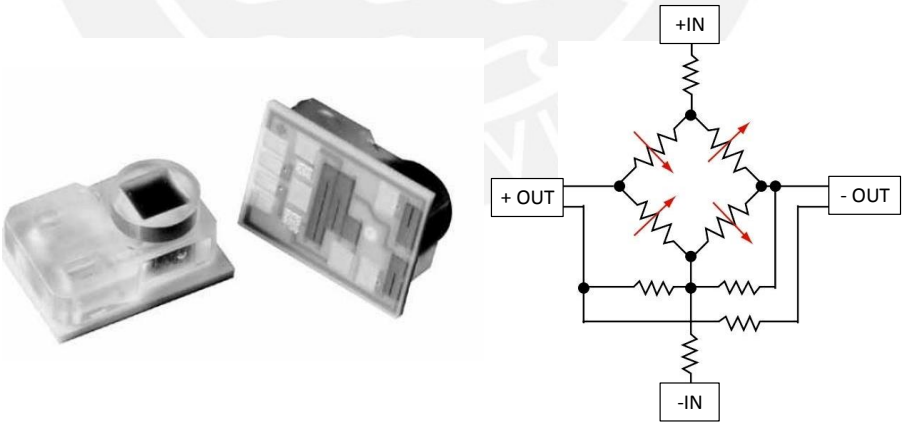

Figure 3.3: NPC-100 (left) Sensor Image (right) Schematic Diagram

Table 3.1: Pressure Sensors

SENSOR CODE	MANUFACTURER	RANGE ($mmHg$)	SIZE ($mm \times mm$)	SENSITIVITY ($\mu V/V/mmHg$)
P161	G.E.	-50 to 300	1.15 x 0.425	12-24
NPC100	G.E.	-30 to 300	8 x 10.41	5
1620	MEAS	-50 to 300	8.13 x 10.54	5
1630	MEAS	-50 to 300	12.7 x 5.08	5

Sensor Signal Conditioner (SSC)

The signal conditioner must accept a full bridge input signal, since not only the selected sensor but mostly all the pressure sensors work in this configuration.

As it was explained before, the signal conditioner will amplify and digitalize the analog signal of the sensor. Since the system is a test module for a future implantable device, the signal conditioner must have low power consumption, good performance in the signal treatment before the processing and a reduced size to ease the system design.

In the table 3.2 some devices which characteristics apply for the design requirements are listed.

Table 3.2: Signal Conditioners

DEVICE CODE	MANUFACTURER	AMPLIFIER RANGE (min-max)	ADC RESOLUTION (bits)	CURRENT CONSUMPTION (μA)
PGA900	Texas Instruments	5-400	24	2600
ZSC3036	ZMDI	13.2-72	16	900
ZSC31014	ZMDI	1.5-192	14	120

The ZSC31014 signal conditioner was selected because of its low current consumption and availability. Another important characteristics are: the device can be configured to work in SLEEP MODE (less current consumption), the digital information can be send via SPI or I^2C and it allows adding an offset value to the digital signal so the sensors range negative part can be processed.The schematic diagram for a full bridge input connection is shown in Figure 3.4.

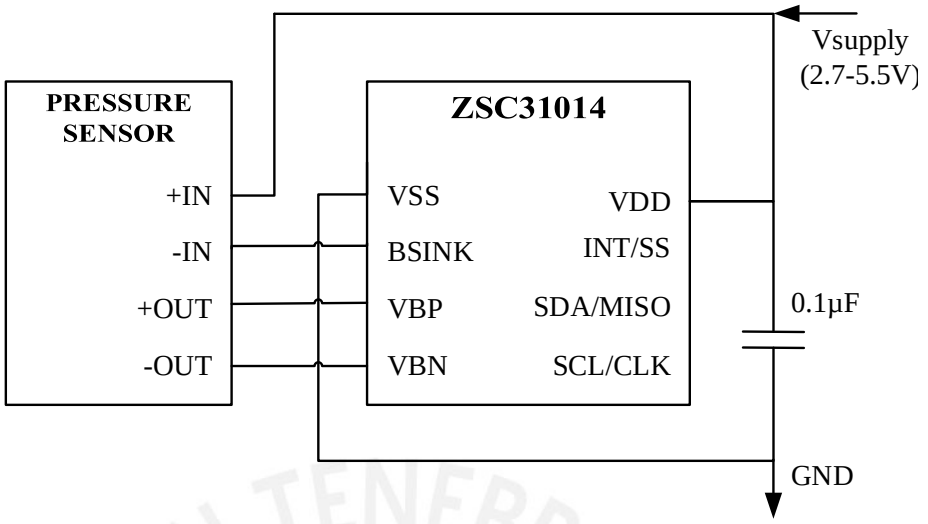

Figure 3.4: ZSC31014 Schematic Diagram

System on Chip

As explained in section 3.1, the system on chip integrates a microcontroller and radio frequency transceiver. The decision to use a SoC, over a microcontroller and RF transceiver separately, was made through the firm determination to make the final system as small as possible and without to much complexity.

For the SoC, the selection criteria was based on the transceiver characteristics of communication. The SoC's RF transceiver must work in the admitted frequency bands for implantable (402 -405 MHz) and medical devices (433 Mhz). Furthermore, the system must have a low power consumption and have USART input/output ports. In Table 3.3 some devices characteristics are compared.

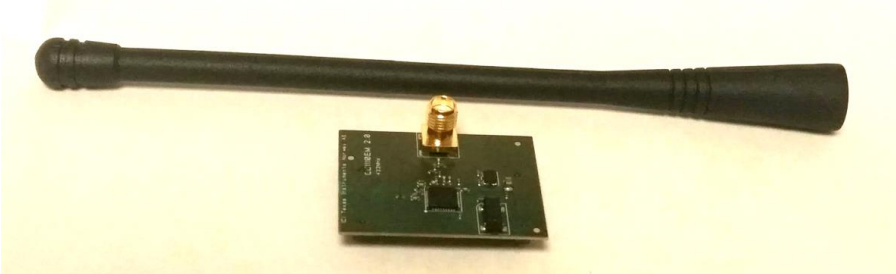

Figure 3.5: CC1110em433

Table 3.3: Systems on Chip with CμC and RF Transceiver

DEVICE CODE	MANUFACTURER	CORE	FREQUENCY RANGES (MHz)	TOTAL MAX. CURRENT CONSUMPTION (mA)
CC1110	Texas Instruments	8051	300 - 348 391-464 782-928	16.2
RF430F5978	Texas Instruments	MSP430	300 - 348 391-464 782-928	15
Si1000	Silicon Labs	8051	240-960	30

Because of its low power consumption and accessibility, the CC1110 Texas Instrument microcontroller is selected. For tests purposes, a CC1110em433 (Figure 3.5), an evaluation module for the selected device, is used.

The evaluation module has already implemented everything necessary to perform a radio frequency communication at 433 MHz.

Serial Communicator

The communication between the SoC and PC is through a serial interface or USB due the high data transfer speed and massive use.

Due to the micro controller does not have a USB peripheral, a UART-USB converter is used. To perform the conversion, the "FTDI basic" (Figure 3.6) is selected. The "FTDI basic" integrates the configuration for a FT232 in a simple and small design.

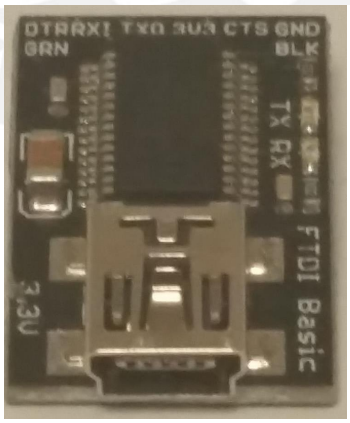

Figure 3.6: FTDI Basic

Implementation

The Figure 3.7 shows the transmitter module's block diagram. As it can be noticed, the module can be powered by three different power supplies, a battery, an external power source and using the "FTDI Basic" (which is connected using a right angle pin header); they can be selected using a switch (POWER SWITCH) which is used to turn off the device too. The pressure sensor can be connected to the module using terminal blocks (PRESSURE SENSOR T.B.).

Furthermore, the communication between CC1110em, ZSC31014 was made using SPI; moreover, the module admits an external device's SPI input that can be connected using a set of terminal blocks (SPI DEVICE T.B.). In the SPI communication the SoC's microcontroller is the master using the USART1 I/O port. Also, for serial communication the SoC microcontroller USART0 I/O port is used. The SoC's pins configuration and the relation between them and the CC1110 evaluation module pins are shown in in the Table 3.4

Finally, the module has output pins in order to measure the important signals, an input for the micro controller debugger that can be used changing the position on two jumpers (JMP and JMP1), and a electromagnetic switch (EM SWITCH) for the battery that can be used changing the position on the jumper JMP2.

Table 3.4: CC1110EM I/O PINS

EVALUATION MODULE PIN	CC1110 I/O PORT	USED AS
4	P1_3	External device Slave Select (CS)
6	P1_1	LED2
7	P0_2	UART0 RX
9	P0_1	UART0 TX
10	P2_1	Debbuger DATA
12	P2_2	Debbuger Clock
13	P1_0	LED1
14	P1_4	ZSC31014 Slave Select (SS)
16	P1_5	SPI Clock
18	P1_6	MOSI
20	P1_7	MISO

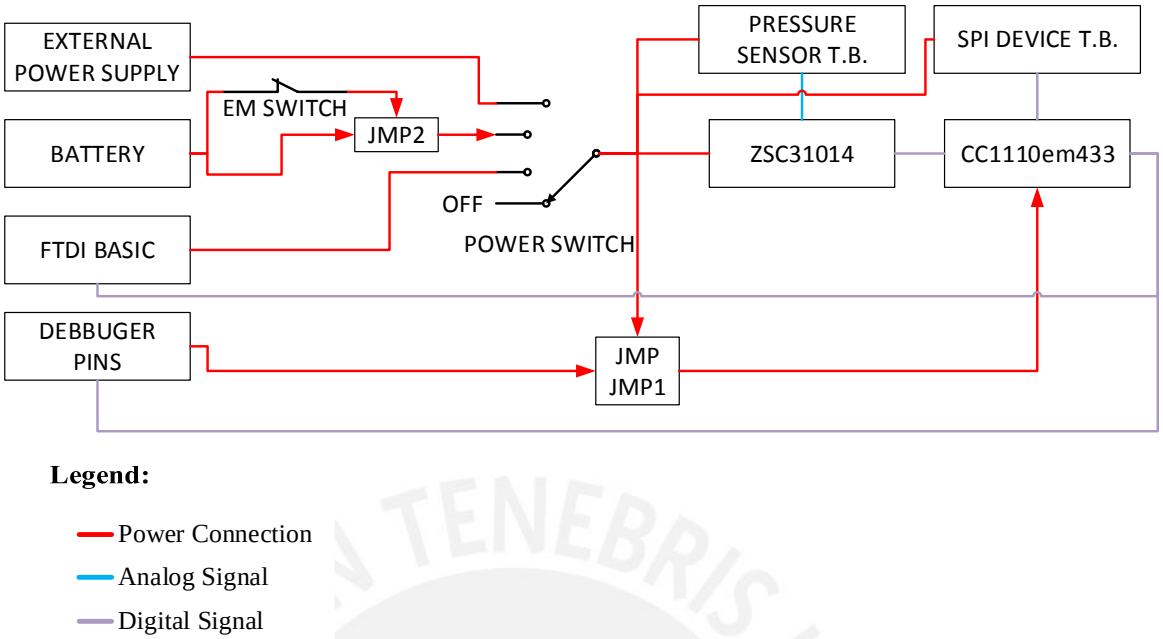

Figure 3.7: Transmitter Module's Block Diagram

The implemented module can be seen in Figure 3.8 and the schematic diagram is shown in the Appendix B.

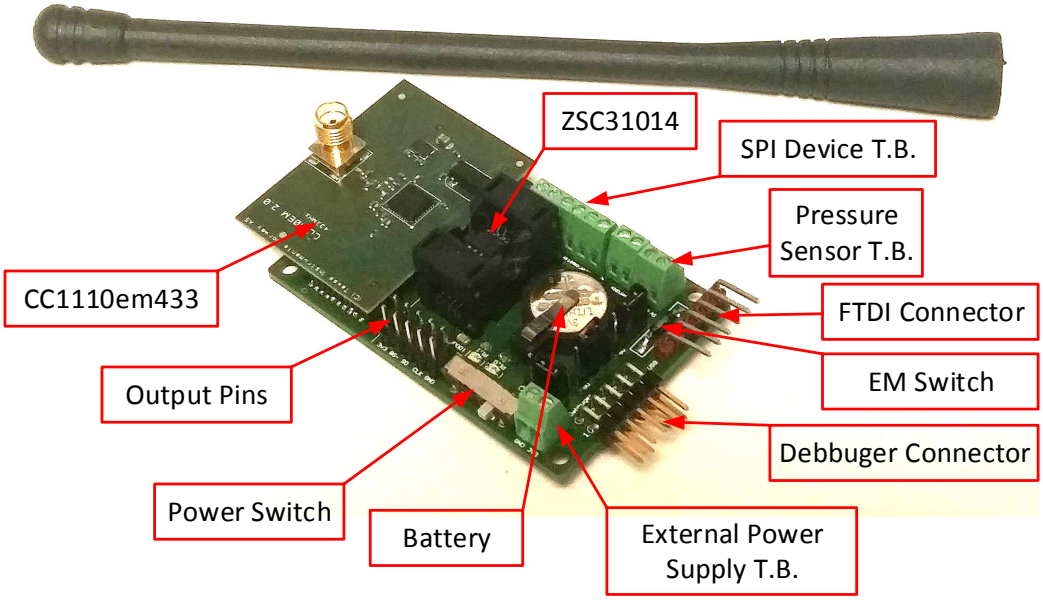

Figure 3.8: Transmitter Module

3.2.2 Receiver Module

The receiver module is based on the CC1110em433, programmed in receive mode. The main function of this module is to be the intermediary between the transmitter module and the PC; to perform this, the SoC is configured tu work using the RF transceiver and one UART I/O port.

Moreover, the receiver module is integrated into the evaluation board SmartRF04eb (Figure 3.9). The evaluation board's function is to give access to the CC1110 UART ports to connect the SoC with the PC by using a serial-USB converter.

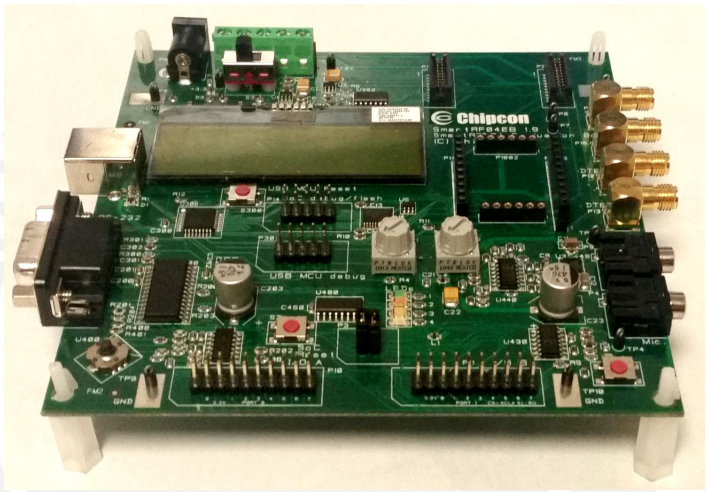

Figure 3.9: SmartRF04eb

4 Graphic User Interface and Communication Protocol

4.1 GUI Development

The GUI was implemented using MATLAB, due the simplicity to perform calculation; despite of the fact, that there are other software, e.g. Labview, better for data acquisition [TLTE12].

The GUI allows the communication with the receiver module. Furthermore, this interface has several function regarding the data administration. Shows the acquired data in real time, allows to save the data in a excel file and allows the sensor calibration.

The developed GUI is shown in the figure 4.1 where three main fields can be appreciated: CONNECTION, CALIBRATION, and DATA HANDLING.

In the CONNECTION field, the user can connect the PC with the receiver module, selecting the proper serial port, and start the data transmission. The data reception algorithm will be explained in section 4.2.3.

In the CALIBRATION field, the user can insert the points taken in order to obtain the sensor calibration parameters, the calibration algorithm will be explained in Section 6.2.2.

Finally, in the DATA HANDLING field, the user has the option to save the data taken on the session into five different data banks; furthermore, the saved data can be plotted and be compared.

For further information about the GUI algorithm, see Appendix C.

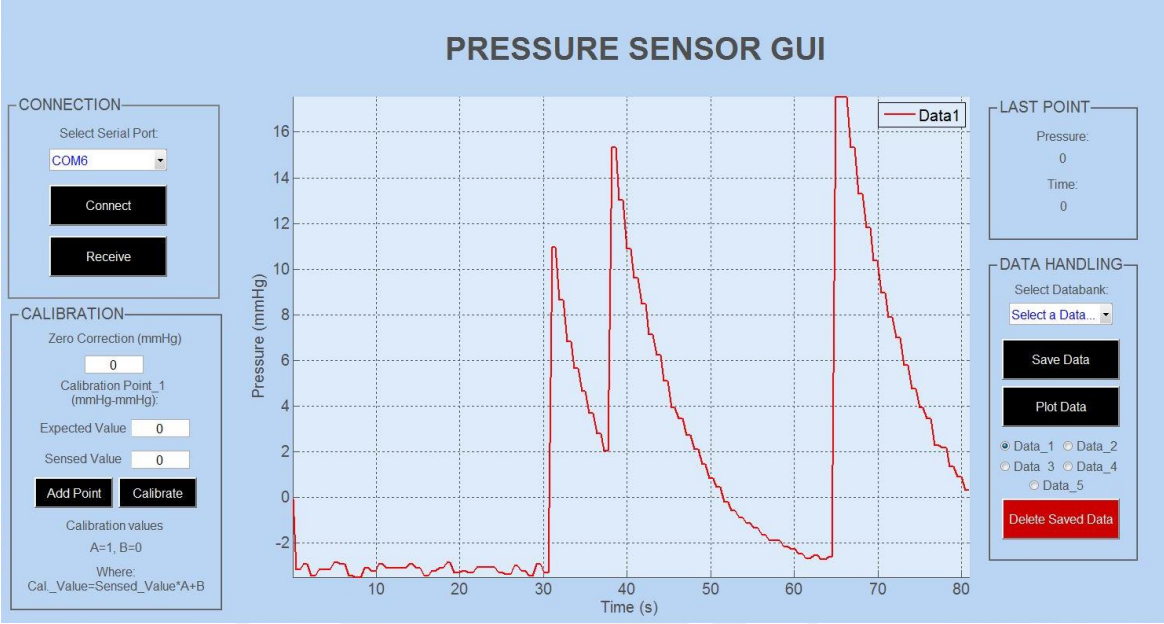

Figure 4.1: Pressure Sensor GUI

4.2 Communication Protocol Development

4.2.1 Communication Block Diagram

The Figure 4.2 illustrates the communication between the system principal devices.

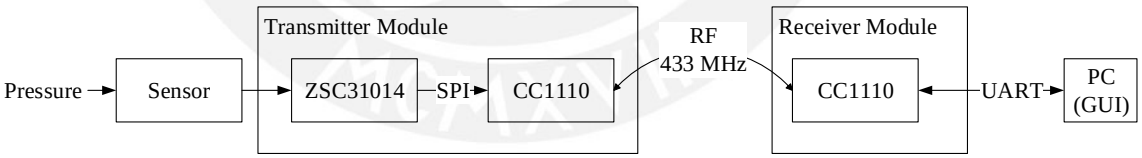

Figure 4.2: Communication Block Diagram

Inside the transmitter module, the communication between the ZSC31014 signal conditioner and the CC1110 μC is performed through the SPI bus; because, the signal conditioner can be configured to work using SPI or I^2C communication; however, the CC1110 μC only have the SPI communication from both options. Furthermore, the

communication is only in one way; due, the SSC only work as a transmitter while on SPI mode.

Both CC1110 radio frequency transceivers will communicate between them using a half duplex, two ways communication; due, both transceivers will send and receive data but only perform an action at a time.

Finally, the communication between the receiver module CC1110 μC and the PC will be performed using the UART peripherals from both devices.

4.2.2 Devices Configuration and Data Packets

SPI Configuration and Data Packets

The ZSC31014 signal conditioner works as a slave when using the SPI communication mode; for this reason, the CC1110 μC was configured in master mode using the USART1 I/O port. Furthermore, the SPI communication will be performed with a 9600 baud rate and negative clock polarity.

The data packet sent by the signal conditioner is by default the one shown in the Figure 4.3, where the sensor information is presented in the fourteen less significant bits of the packet first two bytes.

The device configuration was made using the ZSC31014 evaluation module and "iLite Tester" software provided by the SSC's manufacturer ZMDI. It was initially configured to work in SLEEP MODE, with an Analog Gain of 192 and a 1024 digital offset.

STATUS BITS [7-6]	BRIDGE DATA UPPER BITS [5-0]	BRIDGE DATA LOWER BITS [7-0]	TEMPERATURE UPPER BITS [7-0]	TEMPERATURE LOWER BITS [7-6]	NO RELEVANT BITS [5-0]
1st Byte		2nd Byte	3rd Byte	4th Byte	

Figure 4.3: ZSC31014 Serial Data Packet Format

UART Configuration and Data Packets

The UART settings for the communication between the CC1110 and the PC are shown in the Table 4.1. The data packet sent by the μC is shown in the Figure 4.4, where the first byte contains the data transmitted more significant or upper bits and the second byte the less significant or lower bits. For the UART data request, the PC will send only one byte with the hexadecimal value of 0x24. The receiver module microcontroller USART0 is used to perform this communication.

Table 4.1: UART Configuration

SERIAL PARAMETER	VALUE
Baud Rate	9600
Stop Bits	1
Data Bits	8

START BIT	NO RELEVANT BITS	DATA UPPER BITS	STOP BIT	START BIT	DATA LOWER BITS	STOP BIT
1 Bit	2 Bits	6 Bits	1 BIT	1 BIT	8 BITS	1 BIT

Figure 4.4: UART Data Packet Format

Radio Frequency Configuration and Data Packet

The CC1110 radio frequency transceivers are set to work on the 433 MHz communication base frequency, 1,2 kBaud and 10 dB transmitting power. Furthermore, the transceivers are set to have a four preamble bytes, two synchronization bytes and two CRC bytes to be inserted and removed automatically during transmission and reception respectively.

The radio frequency data packet format is shown in the Figure 4.5, the data packet has a seventeen bytes length field that can be used by the user. In order to secure the data verification, in the first byte the data packet length, and in the next two bytes a network identification are stored.

The last fifteen bytes can be used to store the data to be transmitted. The transmitter module CC1110 will store the sensor information in the first two bytes; while, the receiver module CC1110 will store a request value of 0x2424. The bytes on the free field can be used to send another information in future applications.

PREAMBEL BITS	SYNC BYTES (0xD391)	PACKET LENGTH (0x11)	NETWORK ID (0x5AA5)	USED FIELDS	FREE FIELDS	CRC
4 Bytes	2 Bytes	1 Byte	2 Bytes	2 Bytes	12 Bytes	2 Bytes

Legend:

Inserted automatically in Tx and processed and removed in Rx

Identification provided fields

Used fields for the sensor or request values and free space for another data if necessary.

Figure 4.5: Radio Frequency Data Packet Format

4.2.3 Devices Program Algorithms

GUI Data Reception Algorithm

The GUI data reception algorithm flowchart is shown in Figure 4.6, and the working proceeding is explained below.

When the GUI is in the Receive Stage, the PC sends a request data through the serial port indefinitely until receives and answer. Then, the data read is stored in the serial buffer, waiting for the data validity. If the data is not valid, the program will stop the reception, returning into the Connected Stage and send an error message to the user.

If the data is valid, the program obtain the pressure value from the obtained data (scaling), store the pressure value after the scaling and plot the value versus the time it was obtained. Finally, the program will restart the process to obtain a new pressure value.

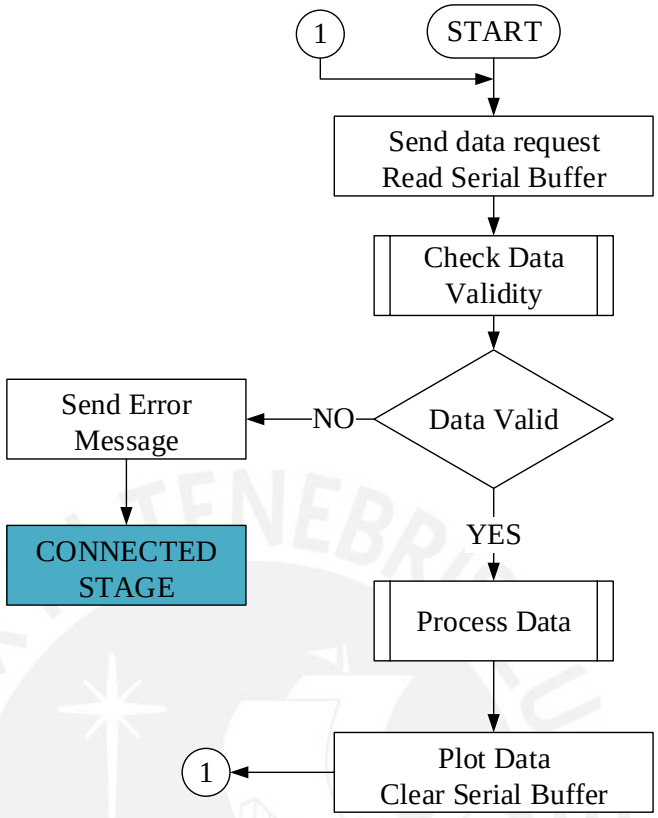

Figure 4.6: GUI Receiver Stage Program Flowchart

Receiver Program Algorithm

The receiver program algorithm flowchart is shown in Figure 4.7, and the working proceeding is explained below.

When the receiver program initializes, it sets the initial parameters for the system on chip microcontroller and radio frequency transceiver as explained before.

Then, the program will enter into a loop, the proceedings done into the loop are explained as follows:

First, the program will activate the USART0 port, read the UART port buffer and store the obtained data from the PC. If the obtained data from the PC is not a valid request value, the program will repeat the proceeding.

Once the obtained data from the PC is a valid request value, the RF transceiver will be set in transmitter mode; then, the request data packet is build and transmitted via RF. The program will wait until the transmission has concluded.

When the transmission has concluded, the RF transceiver will be set in receiver mode and wait until a data packet is received. Once a data packet is received, the validity of the obtained data is checked. If the data is not valid, the program returns and waits to receive another data packet.

Finally, if the data obtained from the RF communication is valid, the data packet relevant bytes are secured. Then the SoC UART0 is activated, the relevant bytes are sent to the PC and the program return to the loop first stage.

The receiver program algorithm flowchart is shown in Figure 4.7.

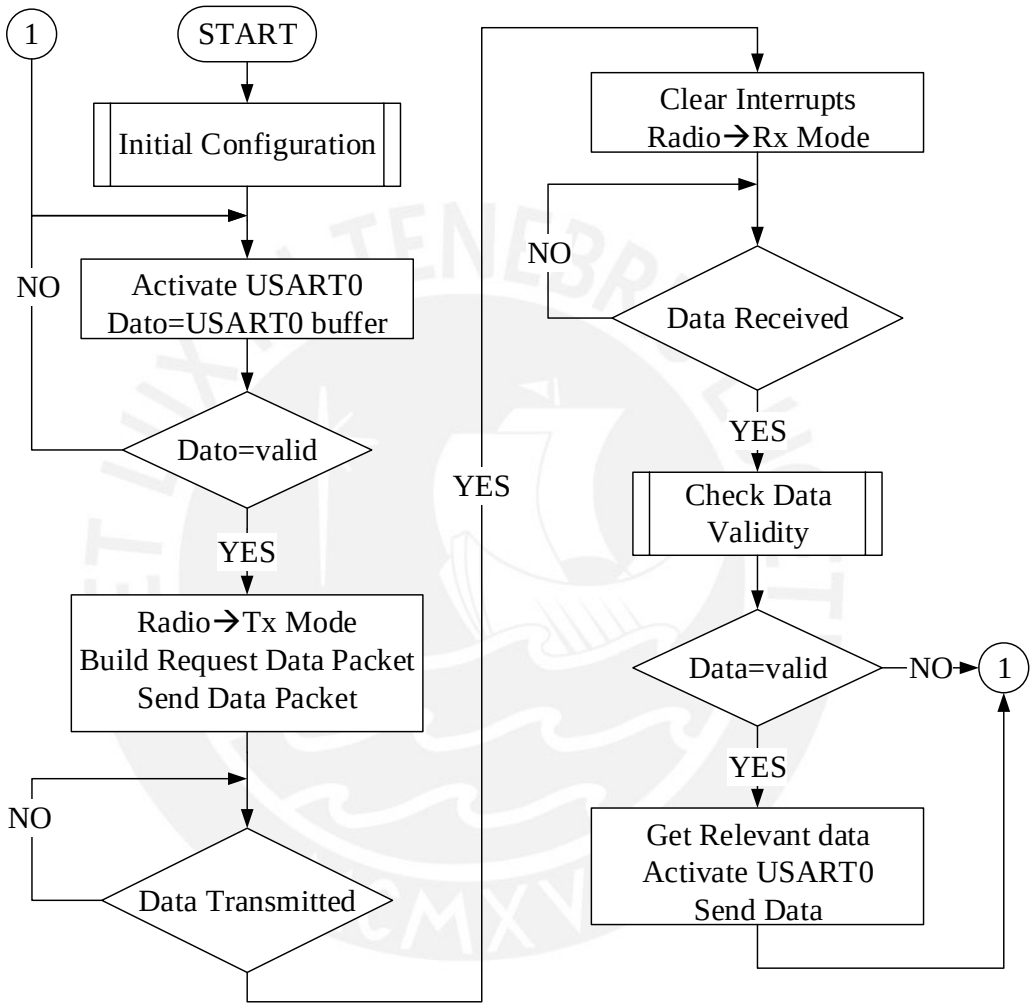

Figure 4.7: Receiver Program Flowchart

Transmitter Program Algorithm

The transmitter program algorithm flowchart is shown in Figure 4.8, and the working proceeding is explained below.

When the receiver program initializes, it sets the initial configuration for the system on chip microcontroller and radio frequency transceiver.

Then, the program will enter into a loop, the proceedings done into the loop are explained as follows:

First, the RF transceiver will be set in receiver mode and wait until a data packet is received. Once a data packet is received, the validity and the value of the data packet is checked. If the data is not valid or the data value is not a request value, the program will return and wait to receive another data packet.

If the data obtained in the previous step is valid and corresponds to a request data, the program will activate the USART1 to work with the SPI configuration and read the MISO input to obtain the reading from the SSC.

Once the data is obtained, the RF transceiver is set in transmitter mode; then, a data packet with the SSC information is build and transmitted. The program will wait until the transmission has finished.

Finally, when the transmission has finished, the program will return to the loop first stage.

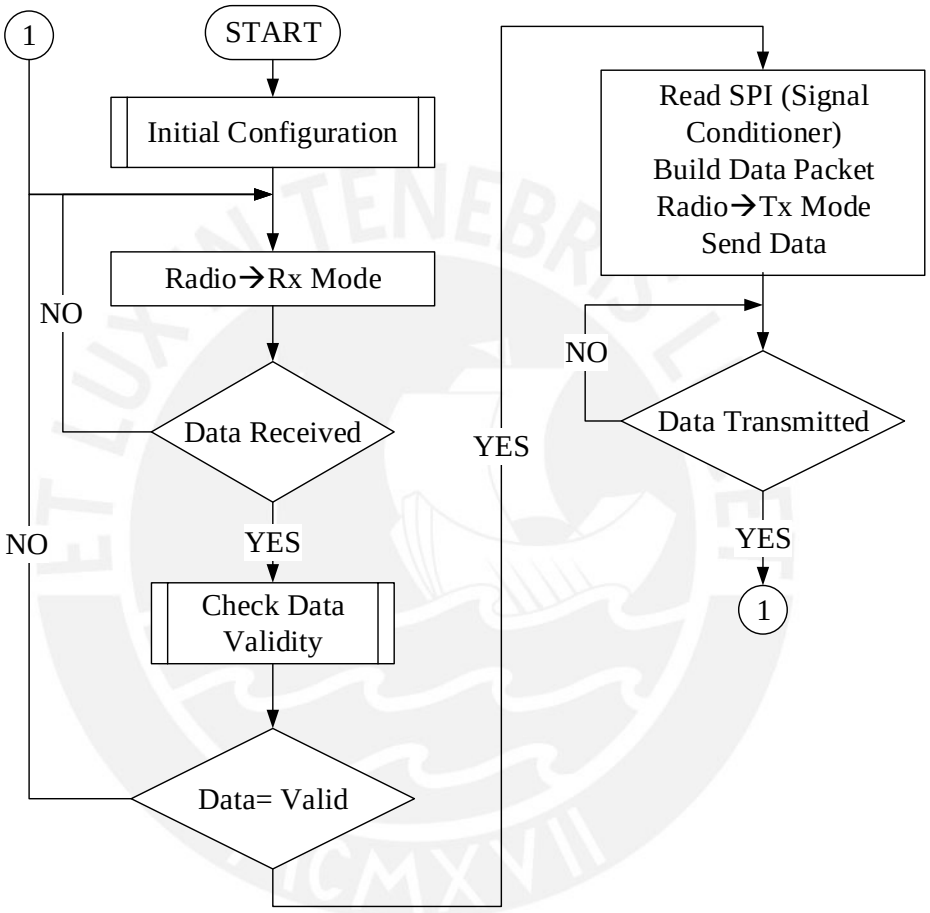

Figure 4.8: Transmitter Program Flowchart

5 Test Bench Implementation

The test bench design was based on an sphygmomanometer way of function; for this, the test bench is consisted by a pressure chamber with two hose connectors and a cable lead-through, a digital manometer and an air pump bulb.

The two hose connectors are used to connect the manometer and bulb hoses hermetically and the cable lead-through is used to let the sensor cables out from the pressure chamber to connect the sensor with the transmitter module.

The Figure 5.1 shows the test bench's schematic and some components of the test bench will be described in the following section.

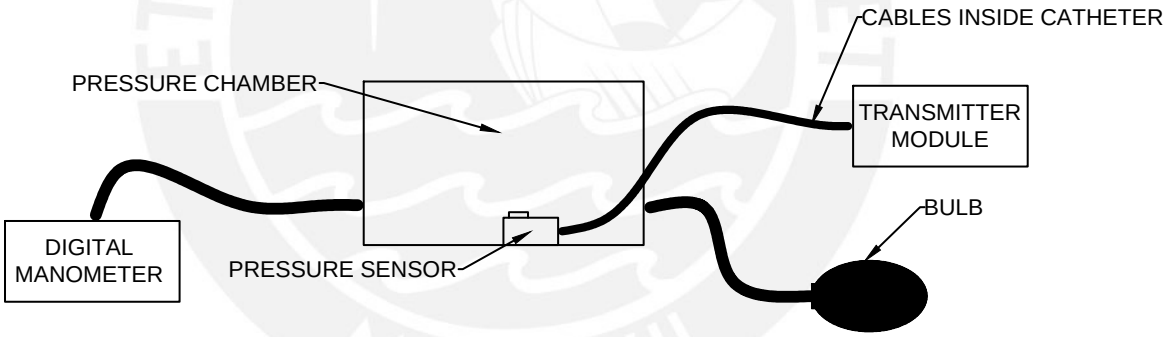

Figure 5.1: Schematic of the test bench setup

5.1 Principal Components Description

5.1.1 Pressure Chamber

Two sealed containers with 250 and 1100 cm^3 capacity were used to implement two different test benches.

This containers were modified to allow the assembly of the hose connectors for the manometer and bulb, and the connection between the sensor and the transmitter module in the container's outside.

The pressure chambers assembly drawings are shown in the Appendix D.

5.1.2 Manometer

A digital manometer is used in the test bench; because; the readings are easier an quicker to make by using a digital device. The Figure 5.2 shows the manometer used in the design.

Furthermore, the manometer used in the test bench has a ±0.3% accuracy; despite of manometers with ±0.2% accuracy are used to calibrate pressure instruments [CS11]. The manometer's accuracy does not have a major effect on the sensor's accuracy after the calibration as shown in Section 6.2.1.

Figure 5.2: Digital Manometer

5.2 Implemented Test Benches

As explained before, to connect the manometer and bulb's hoses, two hose connectors were used. To make the assembly of the connectors with the containers adjusted and hermetic, nuts and O-Rings with the respective diameter were used.

The hose connectors principal dimensions and the O-Rings internal diameters are shown in the Table 5.1.

Table 5.1: Hose Connection Components' Dimensions

HOSE INPUT FROM	HOSE CONNECTOR		O-RING ϕ
	Thread	Internal Hose ϕ	
Manometer	M5	3mm	5 mm
Bulb	G 1/8"	4mm	9mm

Figures 5.3 and 5.4 shows the implemented modules with the two different containers.

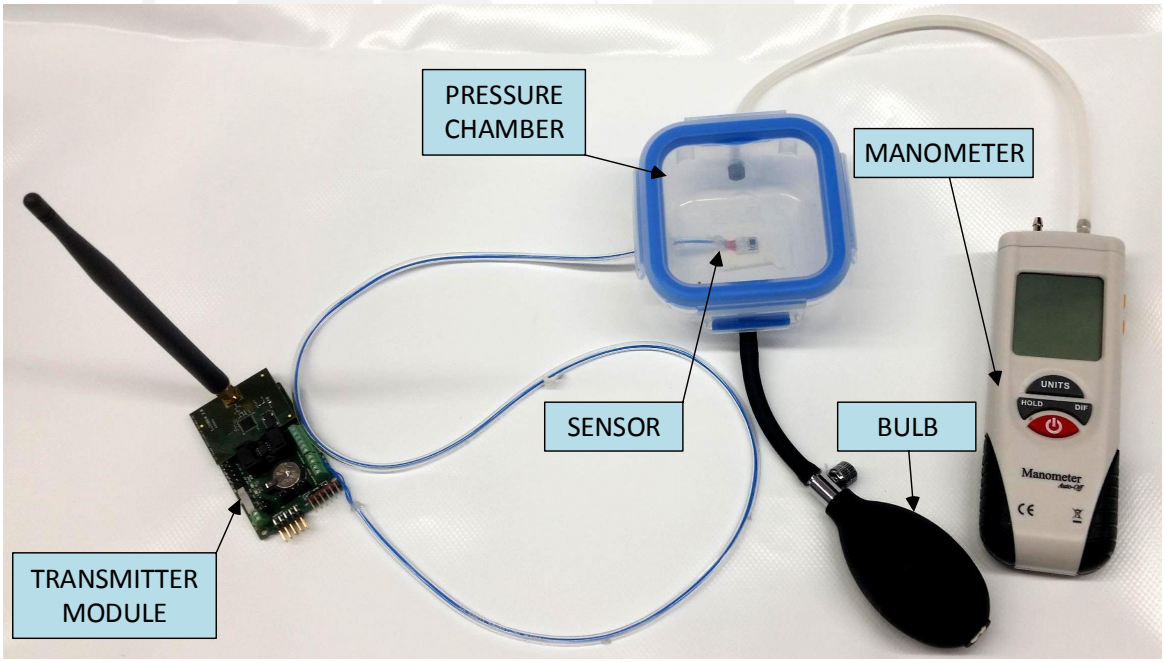

Figure 5.3: Test bench implemented with the 250 cm^3 capacity container

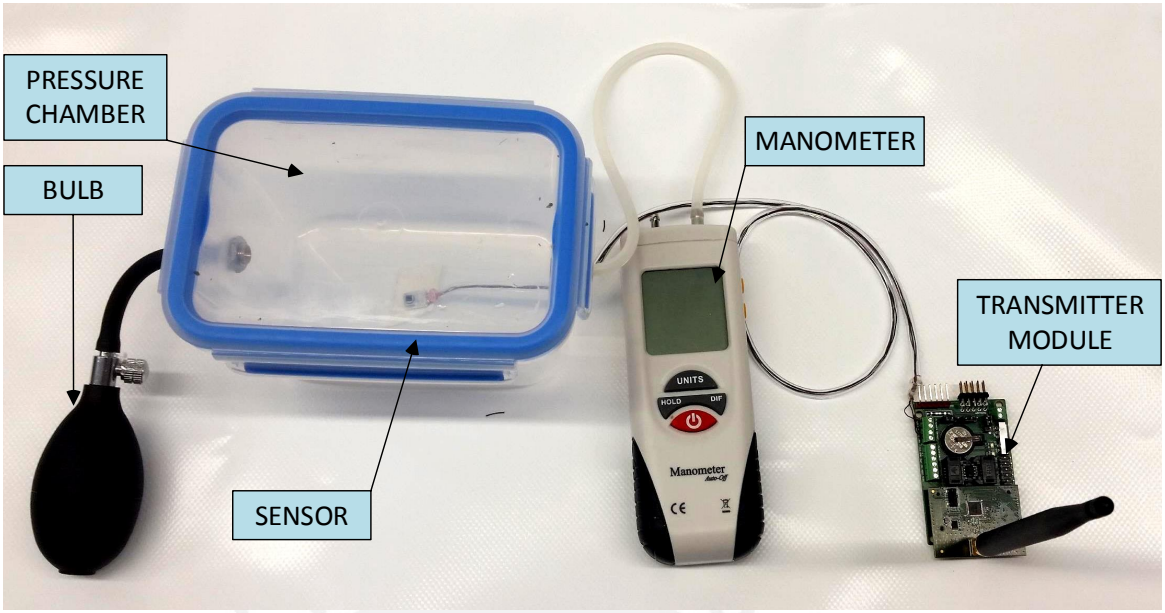

Figure 5.4: Test bench implemented with the 1100 cm^3 capacity container

6 Sensor Calibration and Tests

6.1 Sensor Scaling

To perform the sensor calibration, the Pressure (P) measured in mmHg is needed to be scaled from the digital value given by the signal conditioner (Z). To perform the scaling, the Equations 6.1 and 6.2 are used.

The Equation 6.1 relates P with the voltage drop in the sensor output terminals (V_{out}), where S is the sensor sensitivity and V_{in} the input voltage

$$V_{out} = \frac{P \times V_{in} \times S}{10^6} \tag{6.1}$$

and the Equation 6.2 relates V_{out} with Z and is given in the signal conditioner data sheet (Annex E)

$$Z = 2^{14} \times (GAIN \times \frac{V_{out}}{V_{in}} + A2D\_Offset) \tag{6.2}$$

Finally, solving for the pressure, it is obtained

$$P = (\frac{Z \times 10^6}{2^{14} \times GAIN \times S}) - \frac{A2D\_Offset \times 10^6}{GAIN \times S} \tag{6.3}$$

Using the sensitivity value (S) of $5\mu V/V/mmHg$ given in the Annex A, a GAIN of 192 and A2D_Offset of $\frac{1}{16}$, and replacing this values on the Equation 6.3, it is obtained the relation between the pressure and the digital signal.

$$P \approx (0.0636 \times Z - 65.1)\ mmHg \tag{6.4}$$

6.2 Sensor Calibration

6.2.1 Sensor's Overall Accuracy After Calibration

The calibration of a sensor contribute as a new error source for the sensor accuracy; hence, the sensor's overall accuracy after the calibration is needed to be calculated.

The sensor's overall accuracy after calibrating (O) is the sum of the sensor 's accuracy (S) the overall accuracy of the calibrating instrument (I) and the allowed calibrating tolerance (C) [Stu06]. The Equation 6.5 combines the three sources of error (S, I and C).

$$O = \sqrt{(S)^2 + (I)^2 + (C)^2} \tag{6.5}$$

Then, the sensor's overall accuracy after the calibration, using the sensor and manometer accuracy of $\pm 1\%$ and $\pm 0.3\%$ with a calibrating tolerance of $\pm 0.5\%$ is

$$O = \sqrt{(0.01)^2 + (0.003)^2 + (0.005)^2} = 0.0116 = \pm 1.16\% \tag{6.6}$$

6.2.2 Calibration Method

The calibration method's block diagram is described in the Figure 6.1 and the proceeding is explained as follows.

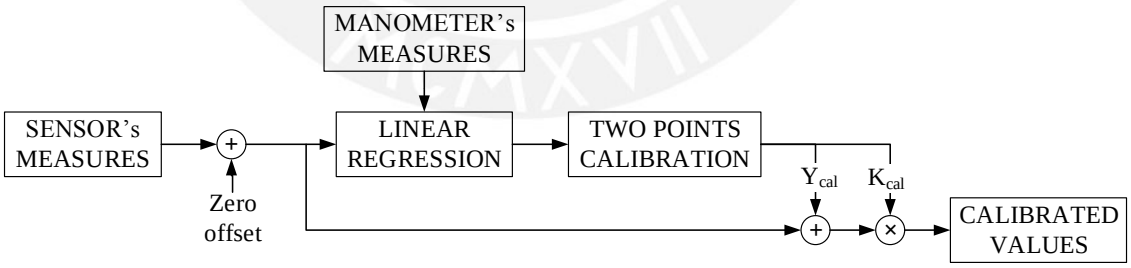

Figure 6.1: Calibration Method's Block Diagram.

The first step to perform the calibration is to take N read points (manometer's read X, sensor's value Y) and the value given by the sensor when the pressure is 0 (Y_0).

To eliminate the sensor's zero offset, Y_0 is used. This value will be subtracted from the sensor values taken (Y) and obtain the values with zero correction as shown in equation 6.7.

$$Y_z = Y - Y_0 \tag{6.7}$$

Then, since the NPC100 is a linear measuring device, the sensor's corrected values (Y_z) with the corresponded manometer's values (X) can be used to estimate a lineal model. The values A and B shown in the equation 6.8 are calculated using the least squares estimation for linear regression.

$$Y_l = A \times X + B \tag{6.8}$$

In addition, a two points calibration is used to correct the slope and the new offset errors; then, the relation between the sensor's calibrated value (Y_f) and the sensor value with zero correction is given in the equation 6.10.

$$Y_f = K_{cal} \times Y_z + Y_{cal} \tag{6.9}$$

Where: $K_{cal} = \frac{1}{A}$ *and* $Y_{cal} = \frac{-B}{A}$

Finally, for every sensor value:

$$Y_f = A_{cal} \times Y + B_{cal} \tag{6.10}$$

Where: $A_{cal} = K_{cal}$ *and* $B_{cal} = Y_{cal} - Y_0 \times K_{cal}$

The calibration method has been implemented to be used with the graphic user interface. In the GUI's CALIBRATION field, the sensor's and manometer's sensed values can be inserted in order to set the comparison points; also, the sensor's zero error can be inserted.

6.2.3 Calibration Results

The calibration of two different NPC100 sensors was performed using the two implemented test benches and under different conditions; because, it was intended to know the sensor response in the two conditions.

Calibration of a sensor without covering

One of the sensors was calibrated without covering and using the small test bench as shown in the Figure 6.2.

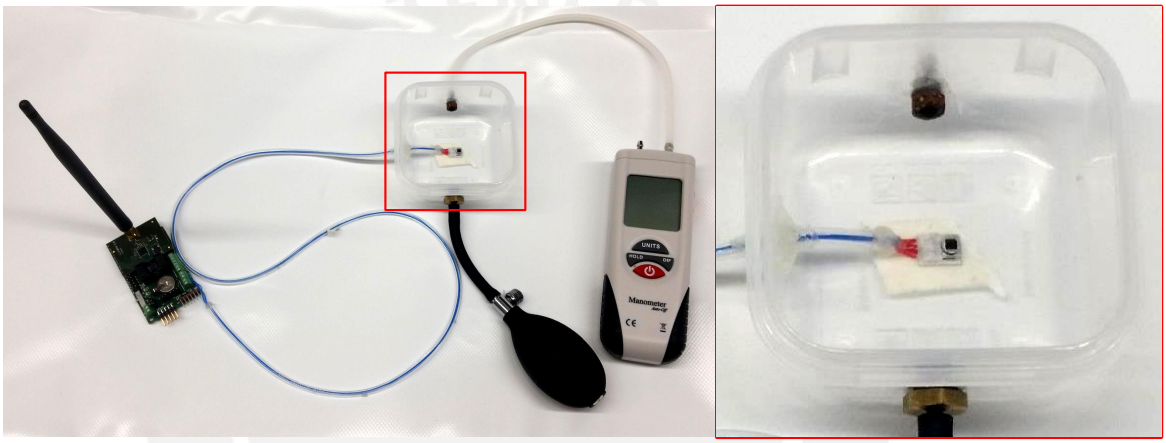

Figure 6.2: Calibration conditions for the first sensor.

The data given by the sensor during the calibration proceeding can be appreciated in the Figure 6.3; also, the sensor's data used for the calibration and the respectively manometer's read are listed in the Table 6.1.

Table 6.1: First sensor's data points taken for calibration

Sensor's Value (mmHg)	-4.93	35.99	39.87	54.74	84.50	92.07
Manometer's Read (mmHg)	0.0	43.9	48.7	59.0	93.6	103.1

Using the implemented calibration method in the graphic user interface the calibration parameters are obtained: $A_{cal} = 1.052$ and $B_{cal} = 5.056$. Then, the corrected sensed

pressure by the NPC100 sensor can be obtained using Equations 6.4 and 6.10.

$$P \approx (0.0669 \times Z - 63.43)\ mmHg \tag{6.11}$$

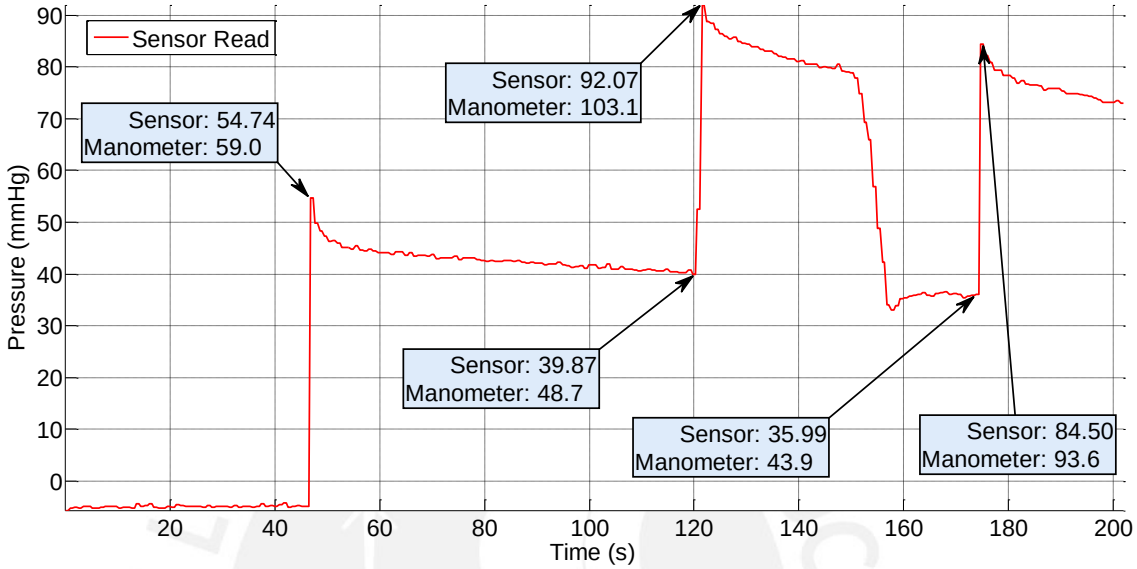

Figure 6.3: Data taken for the calibration of the first sensor.
Pressure (mmHg) vs Time (s).

The Figures 6.4 and 6.5 shows the data points taken, before and after the calibration correction respectively, compared with the sensor expected response.

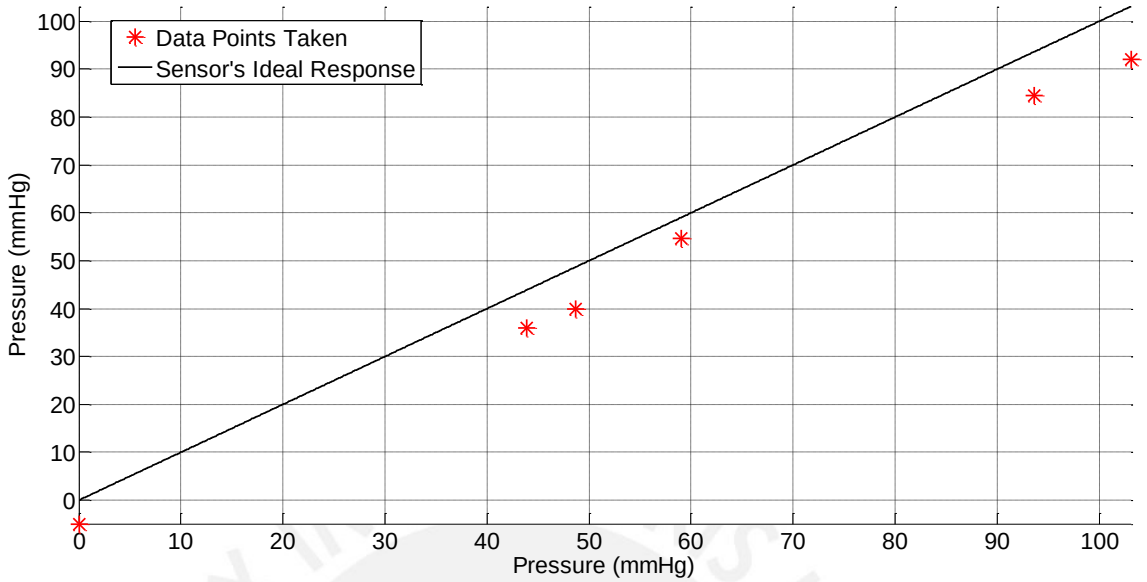

Figure 6.4: Taken data points from the first sensor compared with the sensor's ideal response. Sensor read (mmHg) vs Manometer read (mmHg)

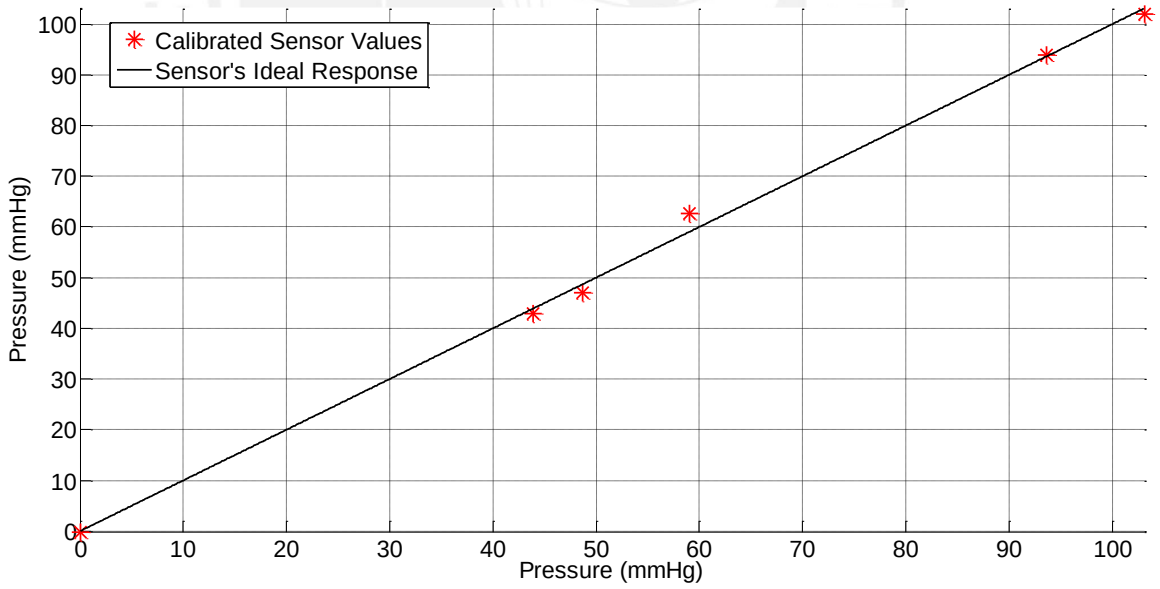

Figure 6.5: Calibrated values from the first sensor compared with the sensor's ideal response. Sensor read (mmHg) vs Manometer read (mmHg)

Calibration of a sensor with silicone covering

The second sensor was calibrated while silicone covered the sensor's body leaving only the sensor's pressure input hole free. The calibration was made using the big test bench as shown in Figure 6.6.

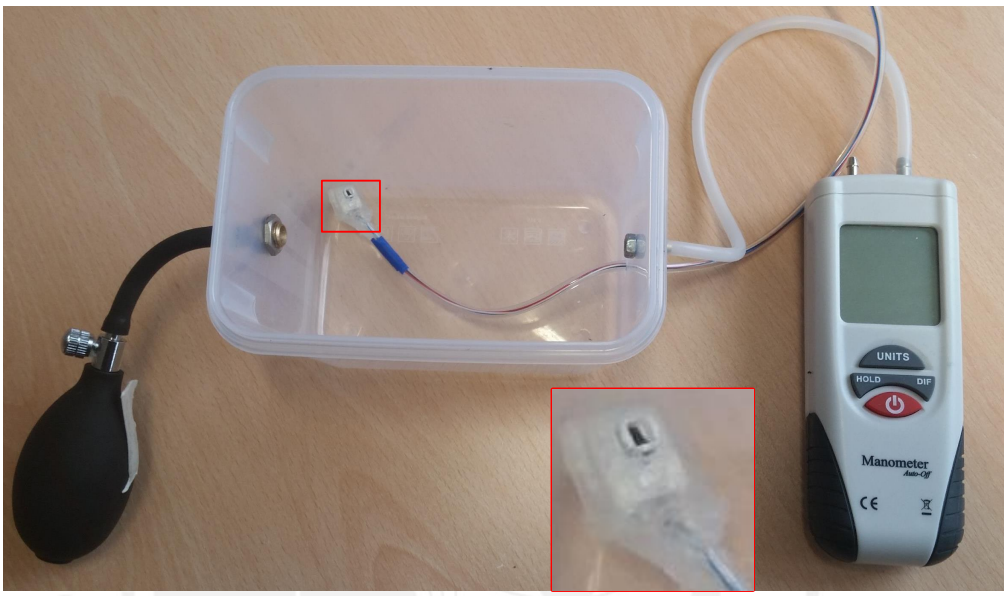

Figure 6.6: Data taken from the NPC100.

The data given by the sensor during the calibration proceeding can be appreciated in the Figure 6.7; also, the sensor's data used for the calibration and the respectively manometer's read are listed in the Table 6.2.

Table 6.2: Second sensor's data points taken for calibration

Sensor's Value (mmHg)	-3.05	-2.07	2.04	10.94	15.32	17.55
Manometer's Read (mmHg)	0.0	0.8	7.1	17.8	24.3	28.2

Using the implemented calibration method in the graphic user interface the calibration parameters are obtained: $A_{cal} = 1.3503$ and $B_{cal} = 3.8675$. Then, the corrected sensed pressure by the NPC100 sensor can be obtained using Equations 6.4 and 6.10.

$$P \approx (0.0859 \times Z - 84.04)\ mmHg \tag{6.12}$$

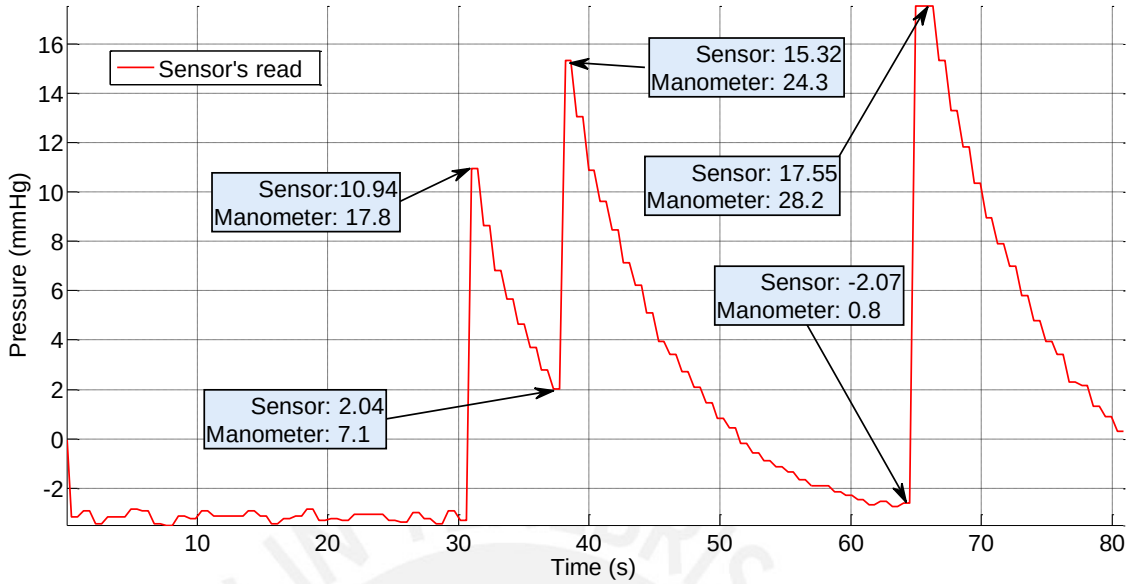

Figure 6.7: Data taken for the calibration of the second sensor.
Pressure (mmHg) vs Time (s).

The Figures 6.8 and 6.9 shows the data points taken, before and after the calibration correction respectively, compared with the sensor expected response.

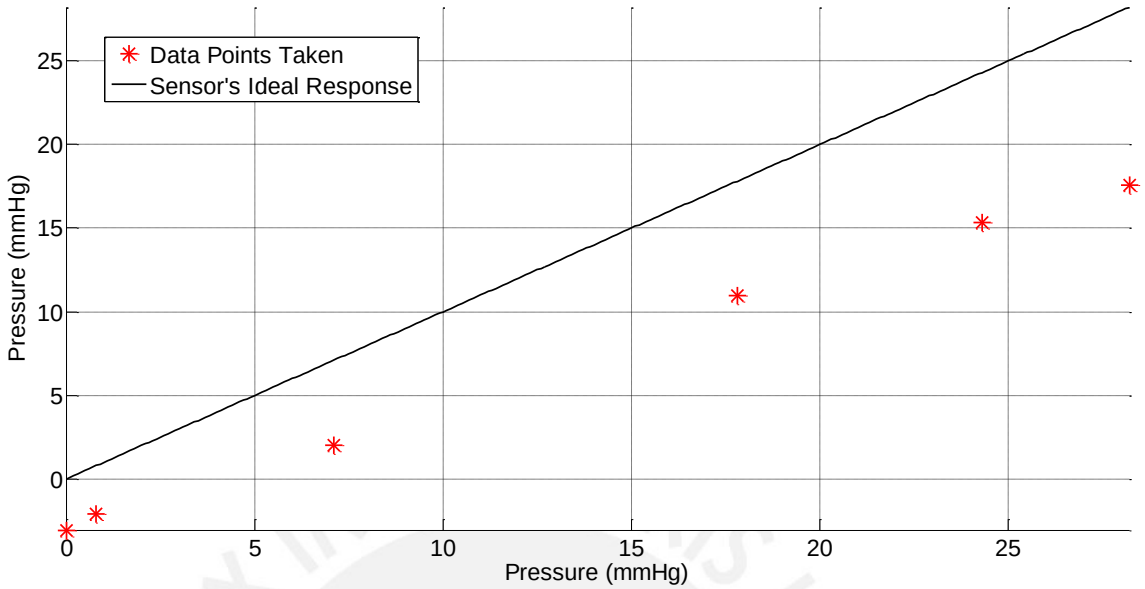

Figure 6.8: Taken data points from the second sensor compared with the sensor's ideal response. Sensor read (mmHg) vs Manometer read (mmHg)

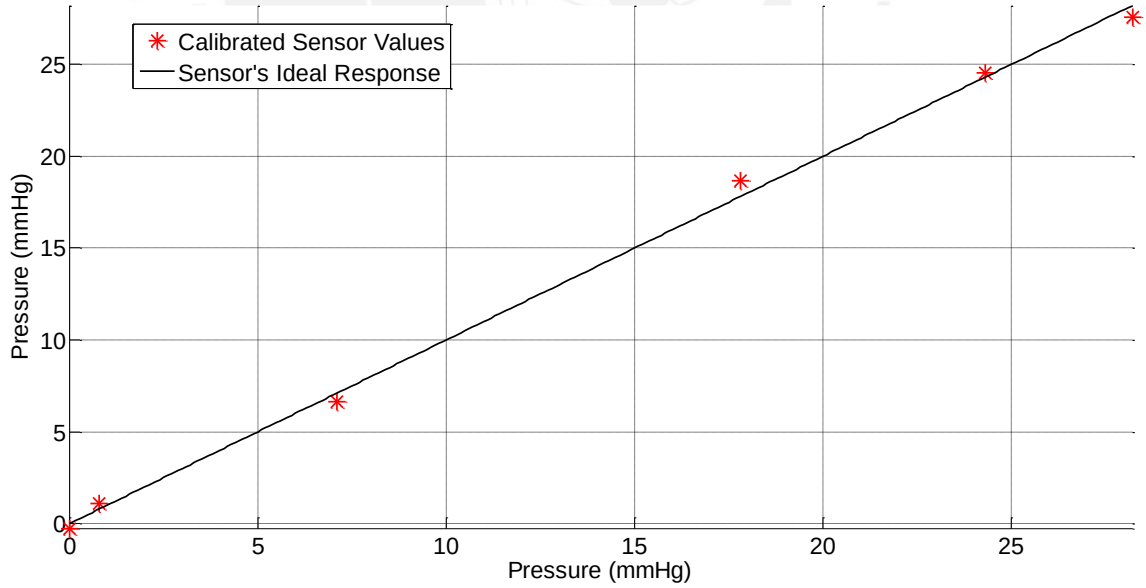

Figure 6.9: Calibrated values from the second sensor compared with the sensor's ideal response. Sensor read (mmHg) vs Manometer read (mmHg)

6.3 Experimental Results

When the sensors calibration had finished, further tests were performed using meat as the sensor environment. This tests were done to calculate the effect of the meat on the sensor readings by comparing pressure measure given by the calibrated sensor with the pressure read given by the manometer.

The sensor was introduced inside a piece of meat as can be appreciated in the Figure 6.10 and then the meat with the sensor were introduced inside the pressure chamber as shown in the Figure 6.11.

The experiments were performed using the two previously calibrated sensors; nevertheless, the two sensors failed after a short period of time while tested.

The Figures 6.12 and 6.13 show the failure of the sensor without and with silicone covering respectively. As ir can be appreciated, the sensor without covering fails in a shorter period of time compared with the covered sensor. This failures could have been produced by the meat humidity.

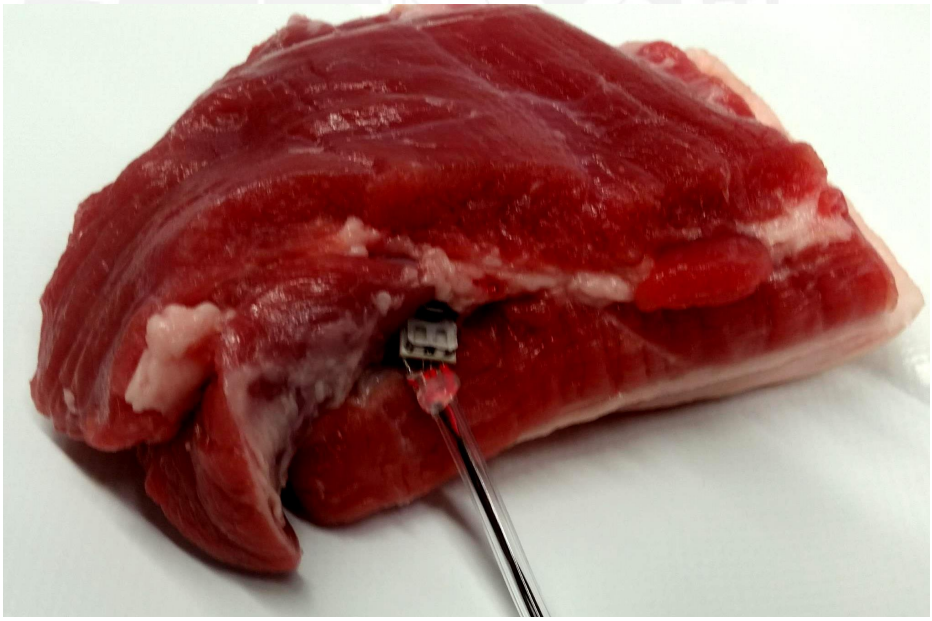

Figure 6.10: Sensor position inside the piece of meat.

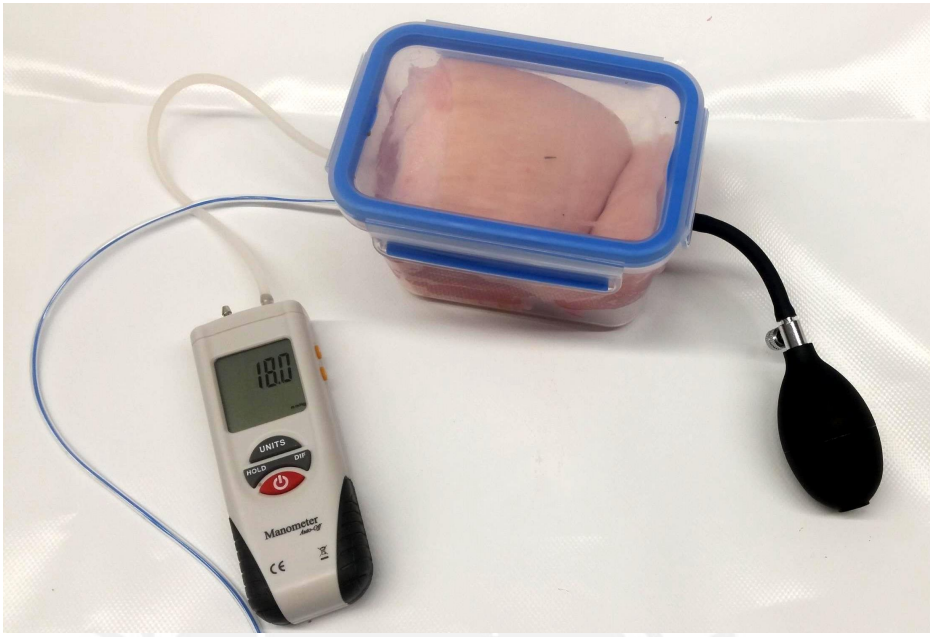

Figure 6.11: Test bench using meat as the sensor's environment

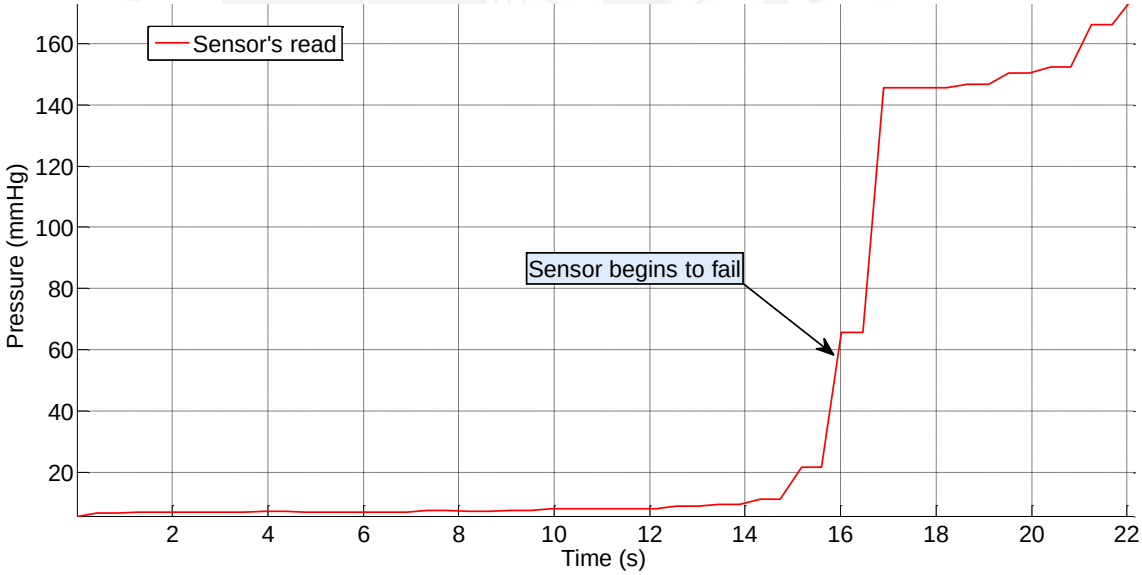

Figure 6.12: Read of the sensor without covering during the test.
Pressure (mmHg) vs Time (s)

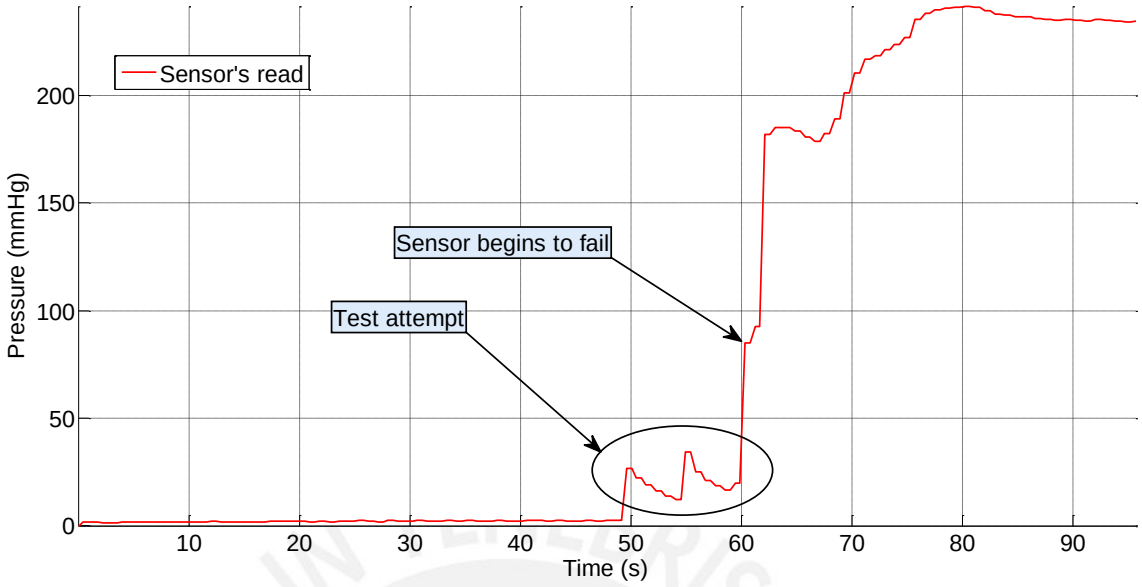

Figure 6.13: Read of the sensor with silicone covering during the test. Pressure (mmHg) vs Time (s)

7 Conclusions and Future Work

7.1 Conclusions

In this work, the design and implementation of a test bench for pressure sensor is presented and validated with practical experiments on a piezoresistive pressure sensor.

The wireless communication system works properly and were designed using low power, small components as it was required; hence, the design of the transmitter module can be used as a reference for the design of the implantable sensing device that will be developed.

In addition, the communication protocol between the communication system modules have been implemented to guaranty the validity of the data and a continuous transmission. Furthermore, the transmitted data is finally shown at real time on the implemented GUI using the MATLAB software on a Windows PC.

Finally, the calibration of the piezoresistive sensors was performed using the implemented test bench system without problems. Nevertheless, when further tests on the sensor were tried to be performed, the sensor begins to fail presumably because of the humidity in the environment where the sensor were tried to be tested.

7.2 Future Work

Future works should be oriented in the design of a covering that will fully protect the selected sensor and perform tests to validate the sensor's capacity for implantation. Furthermore, the design of the implantable sensing device can be performed by using the transmitter module design as reference and a proper antenna to perform the

communication in the radio frequency band for implantable devices of 402-405 MHz.

Bibliography

[AH86] Agostoni, EHER ; Hyatt, RE: Static behaviour of the respiratory system. In: *Handbook of physiology, Section* 3 (1986), S. 113–130

[BHK+96] Brooks, DINA ; Horner, RICHARD L. ; Kozar, LOUISE F. ; Waddell, THOMAS K. ; Render, CAROLINE L. ; Phillipson, ELIOT A.: Validation of a telemetry system for long-term measurement of blood pressure. In: *Journal of Applied Physiology* 81 (1996), Nr. 2, S. 1012–1018

[BJ12] Bazaka, Kateryna ; Jacob, Mohan V.: Implantable devices: issues and challenges. In: *Electronics* 2 (2012), Nr. 1, S. 1–34

[CH05] Caples, SM ; Hubmayr, RD: Respiratory system mechanics and respiratory muscle function. In: *Textbook of critical care. 5th edition. Philadelphia: Elsevier Saunders* (2005), S. 471–82

[Cha04] Chang, Kai: *RF and microwave wireless systems*. Bd. 161. John Wiley & Sons, 2004

[CMI13] Chow, Eric Y. ; Morris, Milton M. ; Irazoqui, Pedro P.: Implantable RF medical devices: the benefits of high-speed communication and much greater communication distances in biomedical applications. In: *Microwave Magazine, IEEE* 14 (2013), Nr. 4, S. 64–73

[CS11] Creus Solé, Antonio: *Instrumentación Industrial*. 2011

[FCMIP91] Fernald, Kenneth W. ; Cook, Todd A. ; Miller III, Thomas K. ; Paulos, John J.: A microprocessor-based implantable telemetry system. In: *Computer* (1991), Nr. 3, S. 23–30

[Gen11] General Electric Company (Hrsg.): *Disposable Medical Pressure Sensor*. General Electric Company, 2011. (TNPC100)

[Har05] Harris, R S.: Pressure-volume curves of the respiratory system. In: *Respiratory care* 50 (2005), Nr. 1, S. 78–99

[KMJD14] Khan, Wahid ; Muntimadugu, Eameema ; Jaffe, Michael ; Domb, Abraham J.: Implantable medical devices. In: *Focal Controlled Drug Delivery*. Springer, 2014, S. 33–59

[KTW+08] Kawoos, Usmah ; Tofighi, Mohammad-Reza ; Warty, Ruchi ; Kralick, Francis A. ; Rosen, Arye: In-vitro and in-vivo trans-scalp evaluation of an intracranial pressure implant at 2.4 GHz. In: *Microwave Theory and Techniques, IEEE Transactions on* 56 (2008), Nr. 10, S. 2356–2365

[LJD+07] Lin, Chihkang C. ; Jea, David ; Dabiri, Foad ; Massey, Tammara ; Tan, Robert ; Sarrafzadeh, Majid ; Srivastava, Mani ; Schulam, Peter ; Schmidt, Jacob ; Montemagno, Carlos: The Development of an In-Vivo Active Pressure Monitoring System. In: *4th International Workshop on Wearable and Implantable Body Sensor Networks (BSN 2007)* Springer, 2007, S. 105–110

[MJJ11] Merrill, DR ; Jeffrey, EA ; Jay, LS: The Electrode—Materials and Configurations. In: *Essential Neuromodulation* (2011), S. 107–152

[PLC05] Park, Chulsung ; Liu, Jinfeng ; Chou, Pai H.: Eco: an ultra-compact low-power wireless sensor node for real-time motion monitoring. In: *Information Processing in Sensor Networks, 2005. IPSN 2005. Fourth International Symposium on* IEEE, 2005, S. 398–403

[RPC+00] Renard, Stephane ; Pisella, C ; Collet, J ; Perruchot, F ; Kergueris, C ; Destrez, Ph ; Rey, Patrice ; Delorme, Nicolas ; Dallard, E: Miniature pressure acquisition microsystem for wireless in vivo measurements. In: *Microtechnologies in Medicine and Biology, 1st Annual International, Conference On. 2000* IEEE, 2000, S. 175–179

[SHR+07] Schlierf, R ; Horst, U ; Ruhl, M ; Schmitz-Rode, T ; Mokwa, W ; Schnakenberg, U: A fast telemetric pressure and temperature sensor system for medical applications. In: *Journal of Micromechanics and Microengineering* 17 (2007), Nr. 7, S. S98

[Stu06] Stum, Karl: Sensor accuracy and calibration theory and practical application. In: *National conference on building commissioning*, 2006, S. 19–21

[TLTE12] Tasner, Tadej ; Lovrec, Darko ; Tasner, Francisek ; Edler, Jörg: Comparison of LabVIEW and MATLAB for Scientific research. In: *Annals of the Faculty of Engineering Hunedoara* 10 (2012), Nr. 3, S. 389

[YK07] Yazdandoost, Kamya Y. ; Kohno, Ryuji: Wireless communications for body implanted medical device. In: *Microwave Conference, 2007. APMC 2007. Asia-Pacific* IEEE, 2007, S. 1–4

Appendix A: NPC-100 Series Specifications

NPC-100 Series Specifications

The NovaSensor NPC-100 Series pressure sensor is specifically designed for use in disposable medical applications. The device is compensated and calibrated per the Association for the Advancement of Medical Instrumentation (AAMI) guidelines for industry acceptability. The sensor integrates a high-performance, pressure sensor die with temperature compensation circuitry and gel protection in a small, low-cost package.

The NPC-100 Series is manufactured in a class 1000 clean-room to minimize possible sources of contamination. A specially designed silicon micromachined sensing element is used to meet or exceed all industry requirements while minimizing assembly and test cost for maximum customer value. Thick-film laser-trimming is employed for final compensation and calibration. Sensitivity is maintained to ±1% and linearity is better than 1% in the physiological operating pressure range.

The NPC-100 Series is batch-manufactured in ceramic plate form and shipped as an intact array for easy customer automation. This assembly method draws from well-established manufacturing techniques used in the electronics industry in order to produce a quality, high volume product.

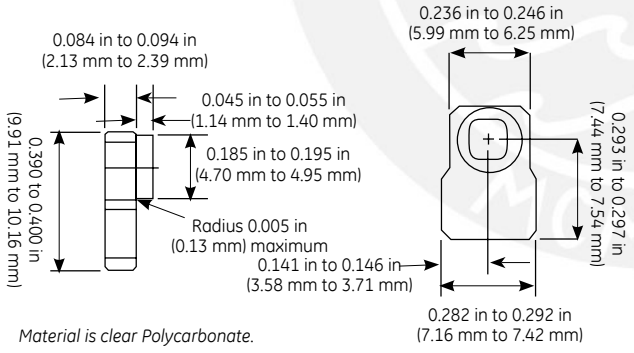

Material is clear Polycarbonate.

NPC-100 Series pressure port interface

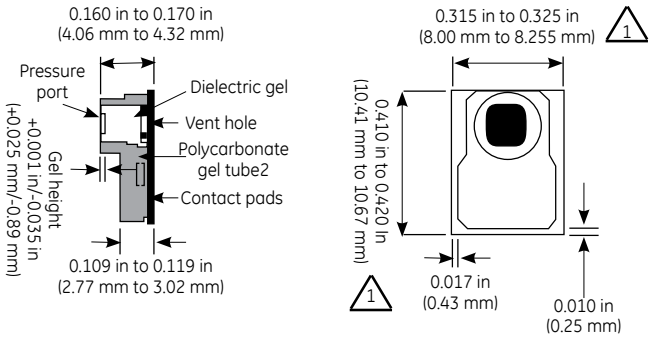

1. Tolerances reflect typical flaring during the singulation process.

NPC-100 Series package diagram

Parameter	Value	Units	Notes
General			
Pressure Ranges	–30 to 300	mmHg	–0.58 psi to 5.8 psi
Overpressure	125	psi	minimum
Electrical @ 72°F (22°C) Unless Otherwise Stated			
Input Excitation	1 to 10	VDC	Calibrated for 6 VDC
Dielectric Breakdown	10,000	VDC	5
Risk Current	2	A	Maximum (per AAMI), 5
Input Impedance	1800 to 3300	Ω	
Output Impedance	285 to 315	Ω	
Environmental			
Temperature			
Compensated	15°C to 40°C	°C	(59° to 104°F)
Operating	15°C to 40°C	°C	(59° to 104°F)
Storage	–25°C to 70°C	°C	(–13° to 158°F)
Humidity	10 to 90	%	
Light Sensitivity	1	mmHg	maximum (per AAMI BP22)
Operating Product Life	168	hours	
Shelf Life	3	years	
Mechanical			
Weight	<0.0044	lb	(<2 g)
Volume Displacement	<0.0008	in^3	(<0.02 mm^3)
Media Interface	Medical grade, dielectric gel		
Gel Tube Interface Material	Polycarbonate		

Parameter	Units	Minimum	Type	Maximum	Notes
Performance Parameters*					
Offset	mmHg	–25	0	25	
Sensitivity	µV/V/mmHg	4.95	5	5.05	
Calibration	mmHg	97.5	100	102.5	2
Symmetry	%	—	—	±5	
Linearity (–30 to 100 mmHg)	mmHg	—	—	1	6
Linearity (100 to 200 mmHg)	% output	—	—	1	6
Linearity (200 to 300 mmHg)	% output	—	—	1.5	6
Thermal Coefficient Offset	mmHg/°C	—	—	±0.3	3
Thermal Coefficient Span	%/°C	—	—	±0.1	3
Frequency Response	Hz	1200	—	—	5
Phase Shift	degrees	—	—	5	5
Offset Drift	mmHg/8 hrs	—	—	1	4,5

** 1. All values measured at 6 VDC and 71.6°F (22°C) and after five second warm up unless otherwise specified.*

2. Output of sensor with no pressure applied and a 150 kΩ resistor shorted across +VIN to +OUT.

3. Over a temperature range of 59°F to 104°F (15°C to 40°C).

4. Normalized offset/bridge voltage—8 hours after 20 seconds. warm-up.

5. Previously qualified, not tested in production.

6. Deviation from straight line drawn through zero and 100 mmHg data points.

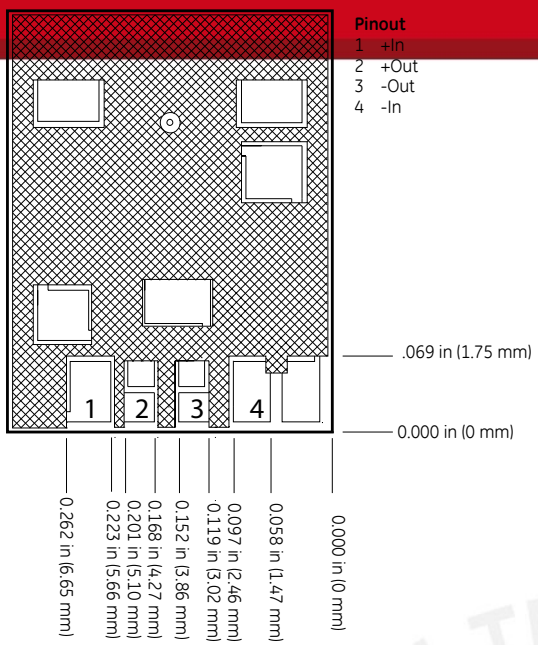

1. *Tolerance on electrical pad location is ±0.010 in (±0.25 mm).*
2. *Contact pads are suitable for soldering.*
3. *Split pads on +Out and –Out must be connected for proper operation.*
4. *All dimensions assume a nominal 0.01 in (0.25 mm) distance between the edge of the solder pads to the edge of the ceramic. This distance will vary slightly from part to part.*

NPC-100 Series electrical interface

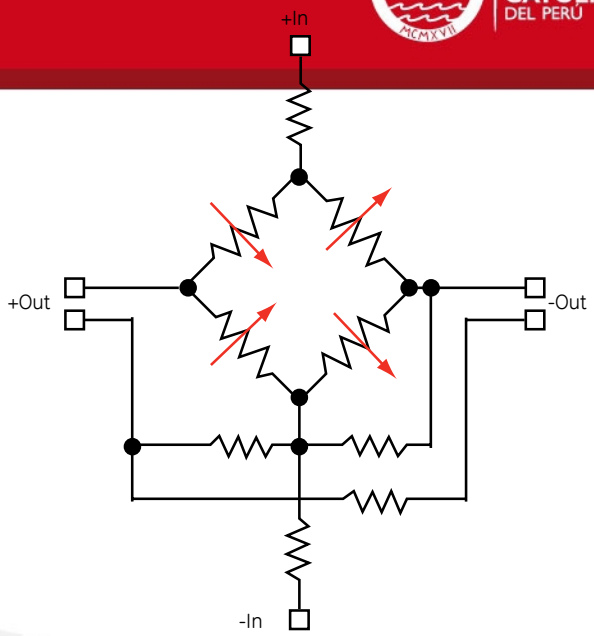

NPC-100 Series schematic diagram

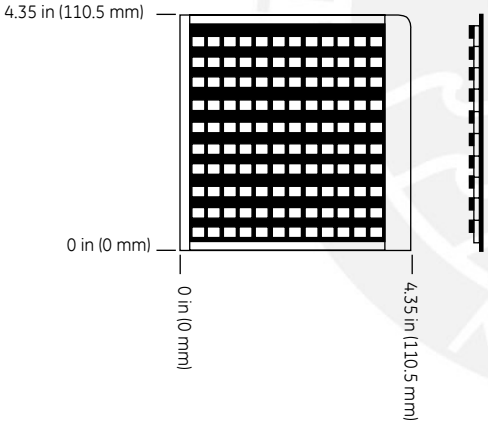

1. *Sensors are shipped as 120 UP snapstrates that must be singulated by the customer.*
2. *Each reel or plate may include units that have failed visual or electrical parameters as well as good units. Bad units are identified with a dot on the backside of the cell location.*
3. *Reels and plates are shipped in dust free anti-static containers to prevent contamination of the gel surface.*

NPC-100 Series shipping Configuration

Warranty

GE warrants its products against defects in material and workmanship for 12 months from the date of shipment. Products not subjected to misuse will be repaired or replaced. GE reserves the right to make changes without further notice to any products herein. GE makes no warranty, representation or guarantee regarding the suitability of its products for any particular application. GE does not assume any liability arising out of the application or use of any product or circuit and specifically disclaims, and all liability, without limitation consequential or incidental damages. The foregoing warranties are exclusive and in lieu of all other warranties, whether written, oral, implied or statutory. No implied statutory warranty of merchantability or fitness for particular purpose shall apply.

Ordering Information

The code number to be ordered may be specified as follows:

NPC-100		
	Code	**Blank: Sold in 120-Up Snapstrate**
	T	Tape and reel
NPC-100 - ___		**Typical model number**

Appendix B: Transmitter Module

Schematic

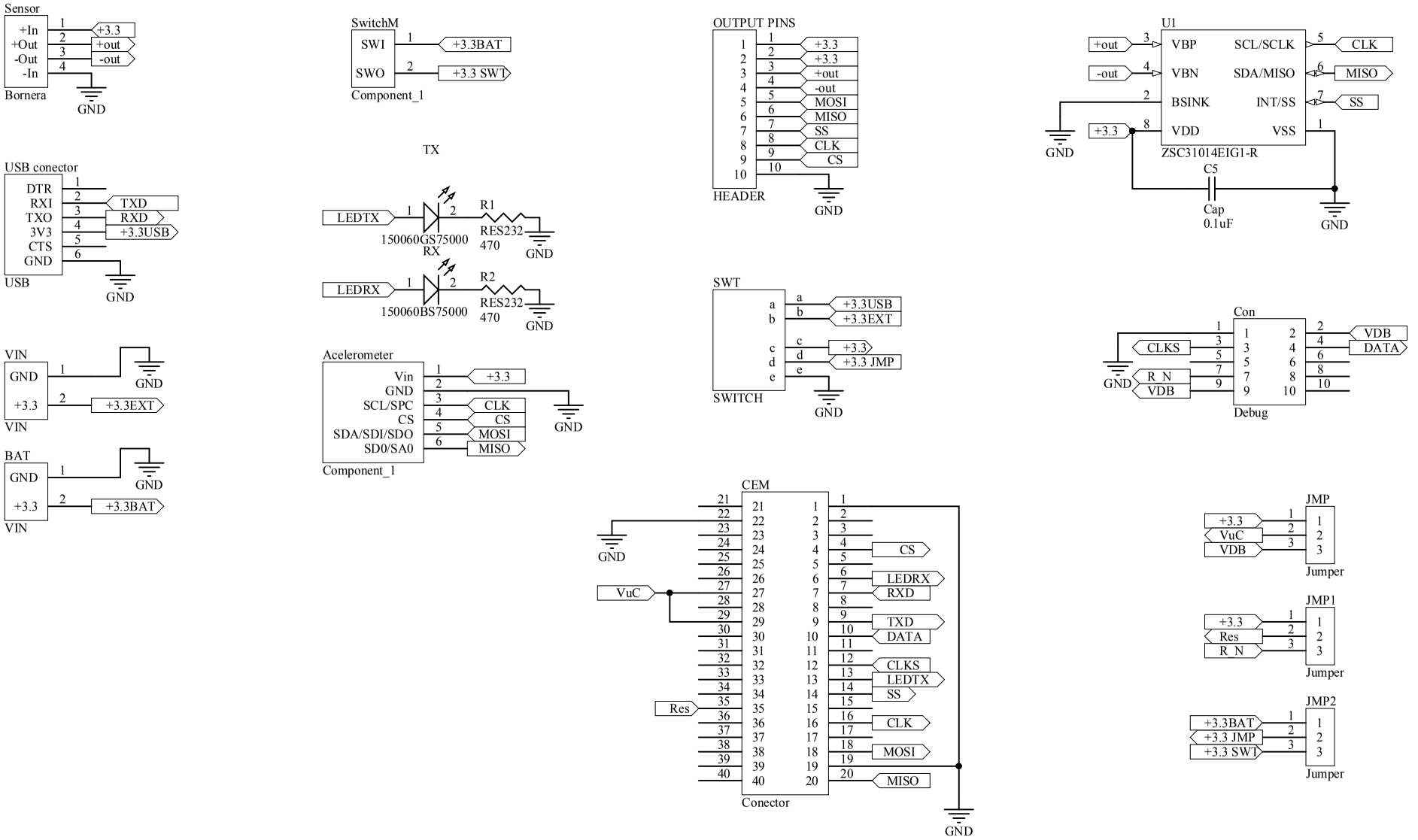

Title: Transmitter Module		
Size: A4	Number:	Revision: 1.0
Date: 10/03/2016		Sheet 1 of 1
File: C:\Users\..\tesis.SchDoc		Drawn By: Antonio Fiestas

Appendix C: GUI Flow Chart

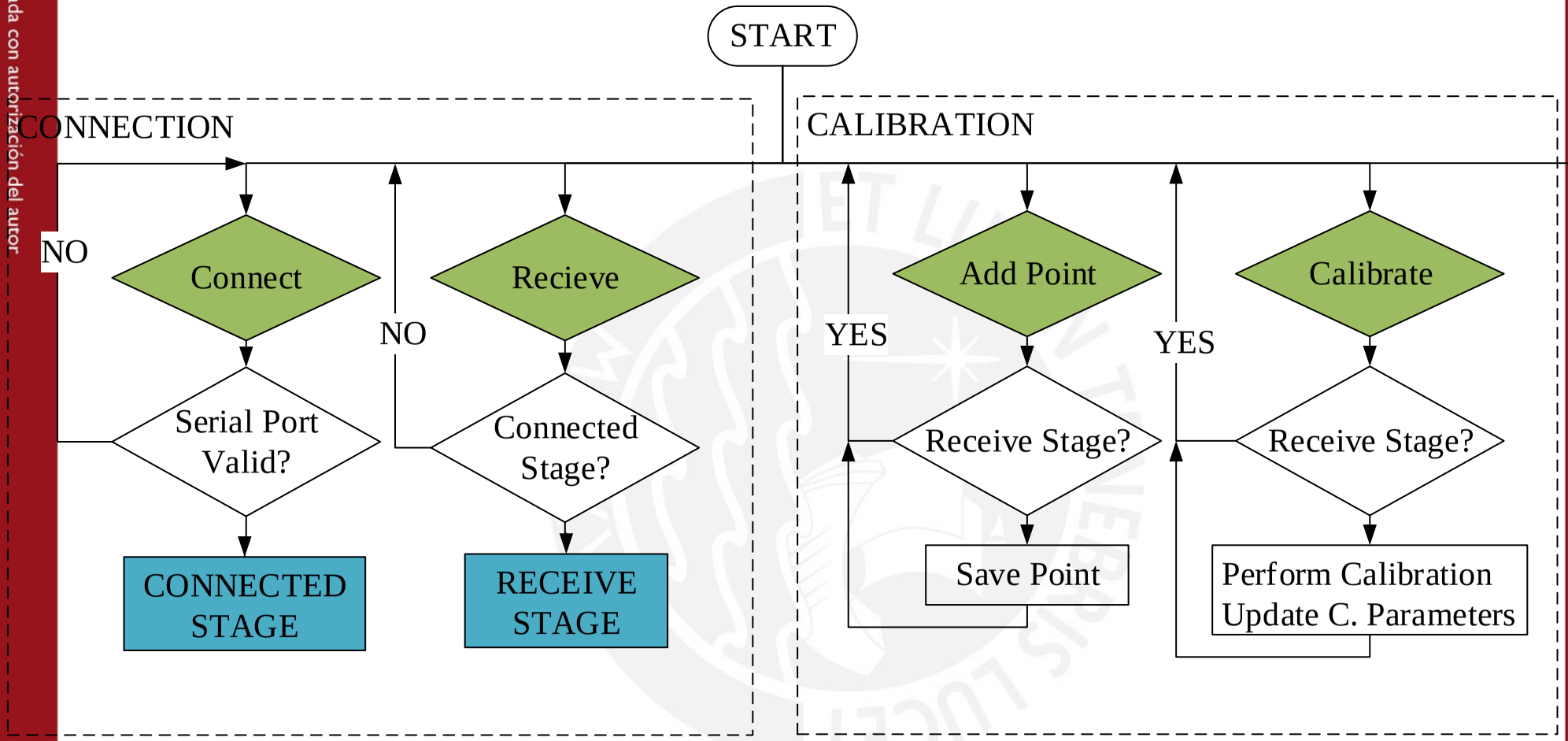

Legend:

- Button Pressed
- GUI stage

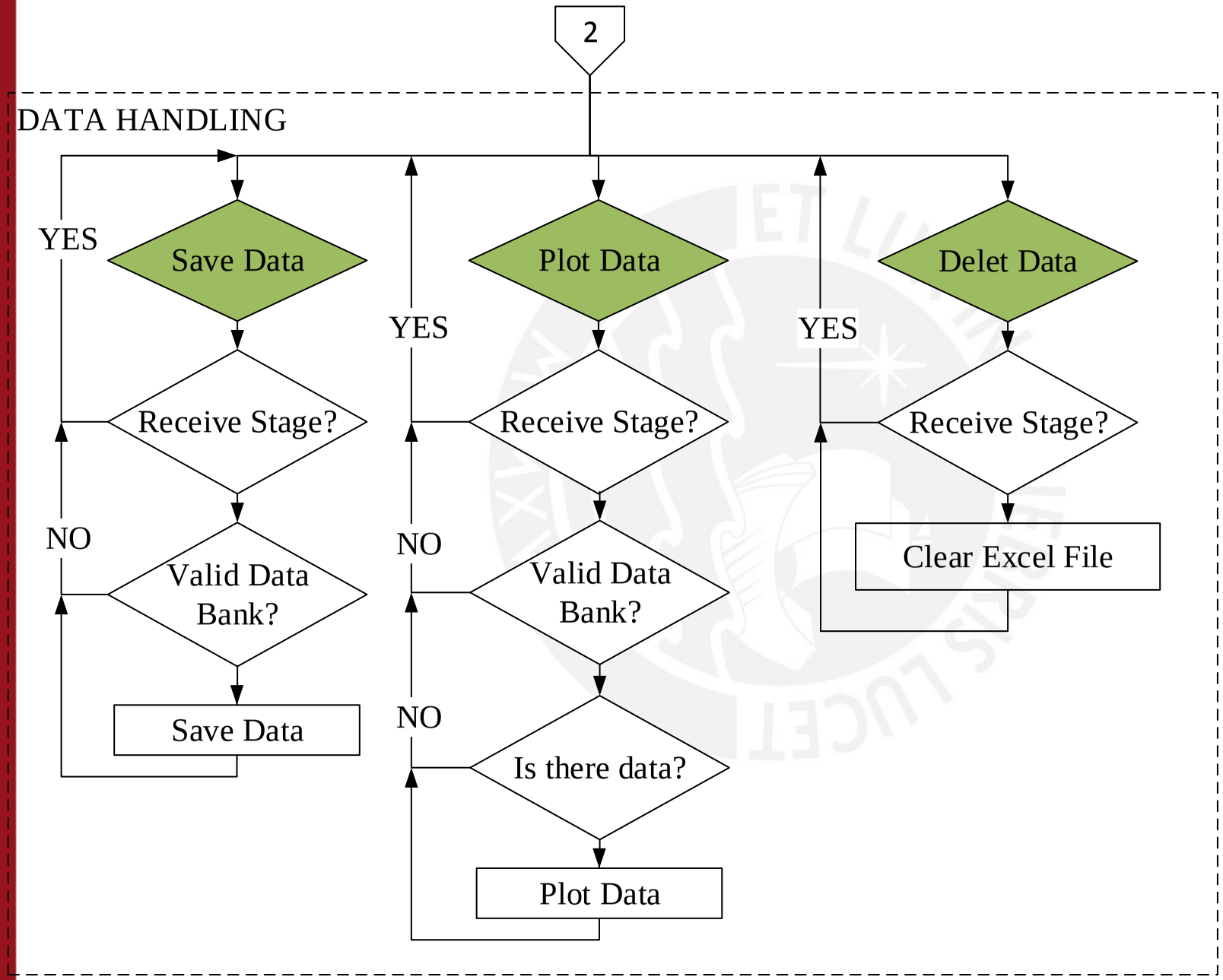

Appendix D: Pressure Chambers

Assembly Drawings

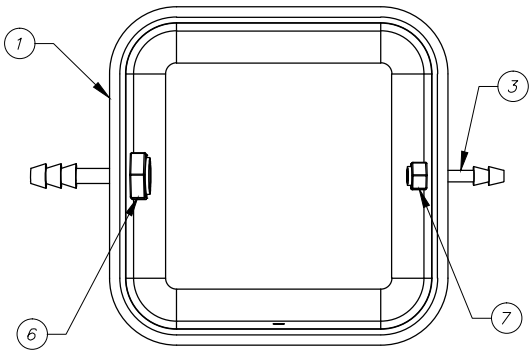

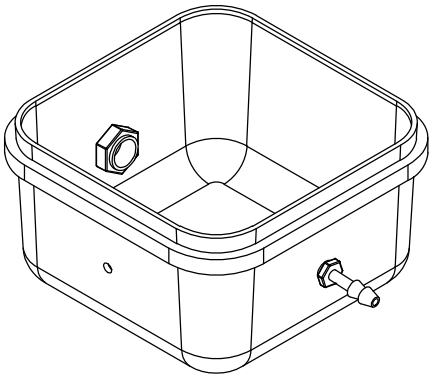

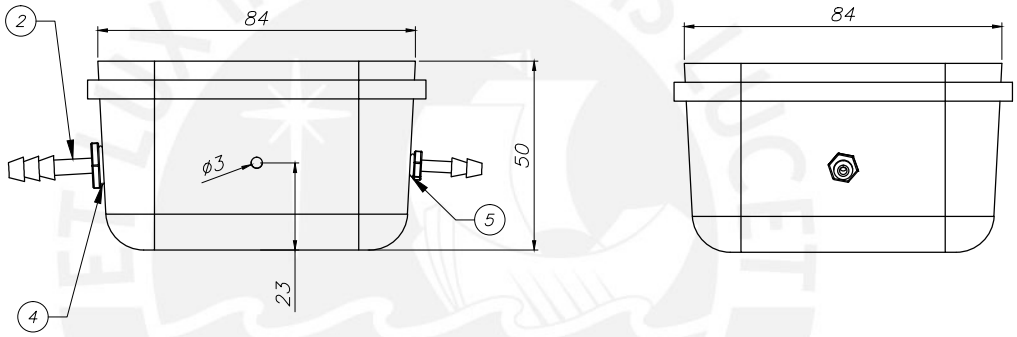

POS.	QTY.	DESCRIPCIÓN	NORMA	MATERIAL	OBSERVACIONES
7	1	Hex nut M5	DIN 934 8.8	ST 37	
6	1	Hex nut G 1/8"	ISO 1175	ST 37	
5	1	O-Ring 5x1N70			
4	1	O-Ring 9x1N70			
3	1	Hose Connector G 1/8"		ST 37	
2	1	Hose Connector M5		ST 37	
1	1	Small Container			

SMALL TEST BENCH CONTAINER

PROYECTION METHOD	MASTER THESIS DESIGN AND IMPLEMENTATION OF A TEST BENCH SYSTEM FOR TRANSFER OF PRESSURE SENSOR DATA	SCALE 1:2
	FIESTAS UGÁS, ANTONIO	DATE: 19/04/2016
		LAMINA: 1/1

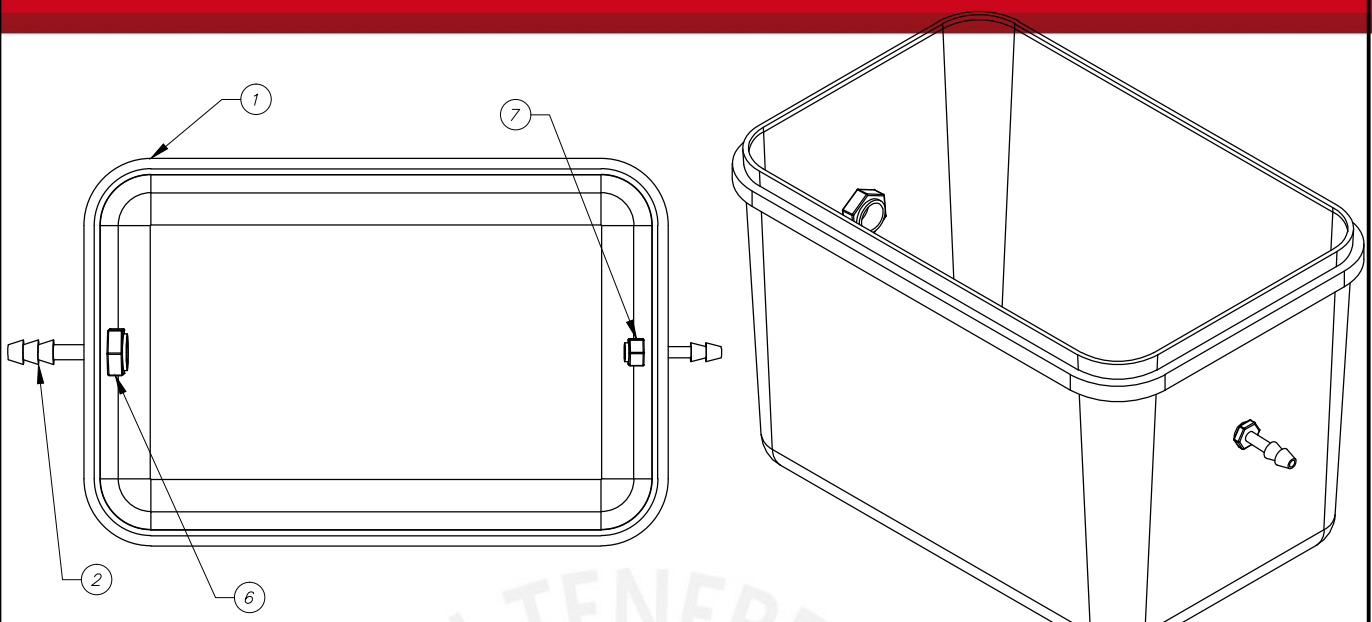

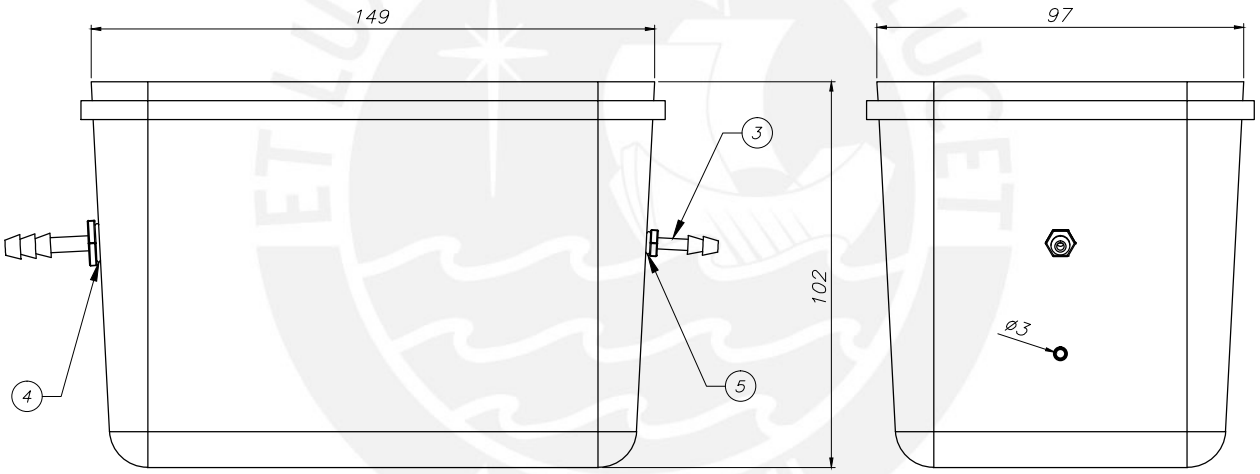

POS.	QTY.	DESCRIPCIÓN	NORMA	MATERIAL	OBSERVACIONES
7	1	Hex nut M5	DIN 934 8.8	ST 37	
6	1	Hex nut G 1/8"	ISO 1175	ST 37	
5	1	O-Ring 5x1N70			
4	1	O-Ring 9x1N70			
3	1	Hose Connector G 1/8"		ST 37	
2	1	Hose Connector M5		ST 37	
1	1	Container			

TEST BENCH CONTAINER

PROYECTION METHOD

MASTER THESIS

DESIGN AND IMPLEMENTATION OF A TEST BENCH SYSTEM FOR TRANSFER OF PRESSURE SENSOR DATA

SCALE 1:2

FIESTAS UGÁS, ANTONIO

DATE: 19/04/2016

LAMINA: 1/1

Appendix E: ZSC31014 Analog Front End

2.2. Analog Front End

2.2.1. Preamplifier (PreAmp)

The preamplifier has a chopper-stabilized two-stage design. The first stage instrumentation-type amplifier has an internal auto-zero (AZ) function in order to prevent the second stage from being overdriven by the amplified offset. The overall chopper guarantees that the whole PreAmp has negligible offset.

There are eight analog gain settings selectable in EEPROM. The polarity of the gain can be changed by shifting the chopper phase between input and output by 180 degrees via the EEPROM setting Gain_Polarity. Changing the polarity can help prevent board layout crossings in cases where the sensor chip layout does not match the ZSC31014 pad/pin layout.

PreAmp_Gain for the bridge measurement is controlled by bits [6:4] in EEPROM Word $0F_{HEX}$ (B_Config register). PreAmp_Gain for temperature is set by bits [6:4] in Word 10_{HEX} (T_Config register). These 3 bits are referred to as [G2:G0]. See section 2.2.3 for recommended temperature measurements settings.

Table 2.1 Preamplifier Gain Control Signals †

G2	G1	G0	PreAmp_Gain
0	0	0	1.5
1	0	0	3
0	0	1	6
1	0	1	12
0	1	0	24
1	1	0	48
0	1	1	96
1	1	1	192

Gain Polarity for the bridge is controlled by bit [7] (Gain_Polarity) in the B_Config register.

Table 2.2 Gain Polarity Control Signal

Gain_Polarity	Overall Gain
0	(-1) ∗ GAIN
1	(+1) ∗ GAIN

† For previous silicon revision A, the available analog gain settings are 1 (G2:G0=000); 3 (G2:G0=100); 5 (G2:G0=001); 15 (G2:G0=101); 24 (G2:G0=010); 40 (G2:G0=011); 72 (G2:G0=110); and 120 (G2:G0=111).

Before a measurement conversion is started, the PreAmp has a phase called nulling. During the nulling phase, the PreAmp measures its internal offset so that it can be removed during the measurement. It is especially useful at higher gains where a small offset could cause the PreAmp to saturate. If bit[12] of the configuration register is set to one, then the nulling feature is disabled as shown in Table 2.3. At lower PreAmp gains, nulling can adversely affect the linearity and ratiometricity of the part, so the recommended setting for this bit is zero for gains of 6 or higher and one for all other gains.

Table 2.3 Disable Nulling Control Signal

Disable_Nulling	Effect
0	Nulling is on
1	Nulling is off

2.2.2. Analog-to-Digital Converter

A 14-bit 2nd order charge-balancing analog-to-digital converter (ADC, A2D) is used to convert signals coming from the PreAmp. By default, each conversion is split into a 9-bit coarse conversion and a 5-bit fine conversion. During the coarse conversion, the amplified signal is integrated (averaged). One coarse conversion covers exactly 4 chopper periods of the PreAmp. A configurable setting stored in EEPROM allows quadrupling the period of the coarse conversion. In Table 3.7, see the LongInt bit in EEPROM words B_Config ($0F_{HEX}$) and T_Config (10_{HEX}). When LongInt = 1, the conversion is performed as 11 bits coarse + 3 bits fine. The advantage of this mode is more noise suppression; however, sampling rates will fall significantly because A2D conversion periods are quadrupled.

An auto-zero (AZ) measurement is performed periodically and subtracted from all ADC results used in calculations. This compensates for any drift of offset vs. temperature. The ADC uses switched capacitor technique and complete full-differential architecture to increase its stability and noise immunity.

Part of the switched capacitor network is a 4-bit digital-to-analog conversion (DAC) function, which allows adding or subtracting a defined offset value resulting in an A2D_Offset shift. This allows for a rough compensation of the bridge offset, which allows a higher PreAmp_Gain to be used and consequently more end resolution of the measured signal. Table 2.4 shows the A2D_Offset adjustment. Using this function, the ADC input range can be shifted in order to optimize the coverage of the sensor signal and sensor offset values as large as the sensor span can be processed without losing resolution.

The A2D_Offset setting for the bridge is controlled by bits [3:0] in Word $0F_{HEX}$ (B_Config). These 4 bits are referred to as [Z3:Z0]. Note: To collect uncalibrated raw bridge values from the ADC, the Offset_B coefficient must be programmed as shown in Table 2.4. Note: The ADC offset for the internal temperature measurement is trimmed at production test to avoid saturation and the setting, which is stored in bits [3:0] in word 10_{HEX} (T_Config), should not be changed (see Table 3.7).

Table 2.4 A2D_Offset Signals

A2D_Offset[3:0]	Auto-Zero Output Count of A2D (+/- 250 Codes)	A2D Input Range [VREF]	A2D_Offset	Offset_B[15:0]
F_{HEX}	15360	-15/16 to 1/16	15/16	$1C00_{HEX}$
E_{HEX}	14336	-7/8 to 1/8	7/8	1800_{HEX}
D_{HEX}	13312	-13/16 to 3/16	13/16	1400_{HEX}
C_{HEX}	12288	-3/4 to 1/4	3/4	1000_{HEX}
B_{HEX}	11264	-11/16 to 5/16	11/16	$0C00_{HEX}$
A_{HEX}	10240	-5/8 to 3/8	5/8	0800_{HEX}
9_{HEX}	9216	-9/16 to 7/16	9/16	0400_{HEX}
8_{HEX}	8192	-1/2 to 1/2	1/2	0000_{HEX}
7_{HEX}	7168	-7/16 to 9/16	7/16	$FC00_{HEX}$
6_{HEX}	6144	-3/8 to 5/8	3/8	$F800_{HEX}$
5_{HEX}	5120	-5/16 to 11/16	5/16	$F400_{HEX}$
4_{HEX}	4096	-1/4 to 3/4	1/4	$F000_{HEX}$
3_{HEX}	3072	-3/16 to 13/16	3/16	$EC00_{HEX}$
2_{HEX}	2048	-1/8 to 7/8	1/8	$E800_{HEX}$
1_{HEX}	1024	-1/16 to 15/16	1/16	$E400_{HEX}$
0_{HEX} 1)	0	0 to 16/16	0	$E000_{HEX}$

1) A setting of 0000_{BIN} for the A2D offset can only be used for internal temperature measurements, which are factory-trimmed (do not change default setting). If it is used for bridge measurements, it could lead to the auto-zero saturating, which results in poor performance of the IC.

Figure 2.2 shows a functional diagram of the ADC. The A/D block at the right side is assumed to be an ideal differential ADC. The summing node B models the offset voltage, which is caused by the tolerance of process parameters and other influences including temperature and changes of power supply. The summing node A adds a voltage, which is controlled by the digital input A2D_Offset. This internal digital-to-analog converter (DAC, D2A) uses binary-weighted capacitors, which are part of the switched capacitor network of the ADC. This DAC function allows optimal adjustment of the input voltage range of the ADC to the amplified output voltage range of the sensor. All signals in this diagram are shown as single-ended for simplicity in understanding the concept; all signals are actually differential. An auto-zero reading is accomplished by short-circuiting the differential ADC input.

Figure 2.2 Functional Diagram of the ADC

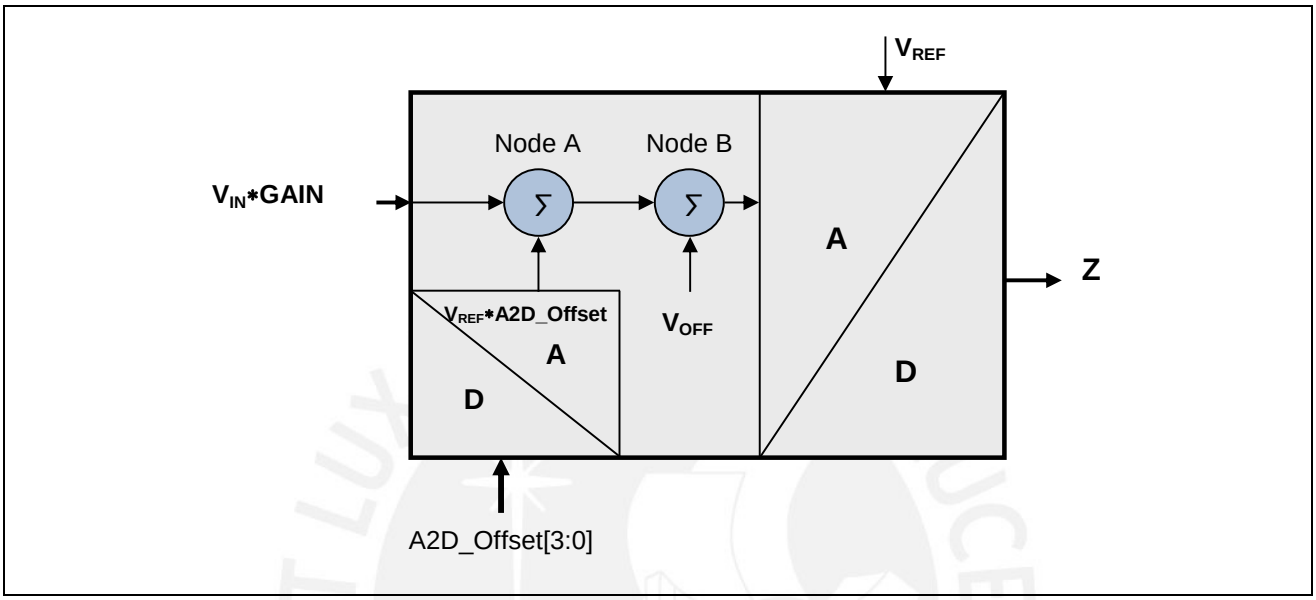

Digital representation of the input voltage as a signed number requires calculating the difference Z_{SENSOR} - $Z_{AUTOZERO}$.

$$Z_{SENSOR} = 2^{14} * (GAIN * V_{IN} / V_{DD} + A2D\_Offset + V_{OFF} / V_{REF}) \quad (1)$$

$$Z_{AUTOZERO} = 2^{14} * (A2D\_Offset + V_{OFF} / V_{REF}) \quad (2)$$

where

GAIN	PreAmp_Gain (B_Config bits [6:4] for bridge measurement; fixed value 6 for temperature measurement) (See Table 2.1)
A2D_Offset	Zero Shift of ADC (B_Config or T_Config bits [3:0]) (See Table 2.4)
V_{REF}	~ V_{DD} Supply Voltage to ZSC31014
V_{IN}	Input Voltage = (V_{BP}-V_{BN}) in differential mode; = (V_{BP}-V_{DD}/2) in half-bridge mode
V_{OFF}	Small random offset voltage that varies part-to-part and with temperature. The periodic auto-zero cycle will subtract this error.

The digital output Z as a function of the analog input of the analog front-end (including the PreAmp) can be described as

$$Z = Z_{SENSOR} - Z_{AUTOZERO}$$

$$Z = 2^{14} * (GAIN * V_{IN} / V_{REF}) \quad (3)$$

With $V_{REF} = V_{DD} - V_{BSink}$ (see section 2.2.4) where V_{BSink} is the voltage at the BSINK pin.

2.2.3. Temperature Measurement

The temperature signal comes from an internal measurement of the die temperature. The temperature signal is generated from a bridge-type sensor using resistors with different TC values. Table 2.5 shows the characteristic parameters. This temperature signal can be corrected with offset, span, and 2nd order non-linearity coefficients. The corrected temperature can then be read on the digital output I²C™ or SPI with either an 8 or 11 bit resolution. The raw temperature reading can also be used to compensate the sensor bridge reading. 1st order Tco and Tcg, and 2nd order Tco and Tcg coefficients are available to correct sensor bridge offset and span variations with temperature.

Table 2.5 Parameters of the Internal Temperature Sensor Bridge

Parameter	Min	Typ	Max	Units
Sensitivity	0.28	0.38	0.5	mV/V/K
Offset voltage	-75		65	mV/V
Nonlinearity (-20 to 80°C) first order fit			2	°C
Nonlinearity (-20 to 80°C) second-order fit			0.25	°C
Bridge resistance	15	20	25	kΩ

NOTE: The T_CONFIG register description is given in section 2.2.5. Most fields within this EEPROM register are programmed to default settings on the production test and should not be changed. Only the LongInt field (bit 8) setting is user-selectable if desired. Other settings for the remaining T_Config bits might cause temperature measurements to saturate. Section 2.2.5 gives the details of how PreAmp_Gain and A2D_Offset Mode are configured for temperature measurements.

For ZSC31014 SOP8-packaged parts, the on-chip temperature sensor is calibrated by ZMDI using three temperature points: -40°C, room temperature (RT), and +85°C, which provides a 2nd-order fit. The error of the conditioned temperature output data at delivery is specified as ≤ 2.5 Kelvin over the full operational temperature range of -40 to +125°C.

Note: This calibration causes a change in the EEPROM default data in the EEPROM registers $0A_{HEX}$ to $0D_{HEX}$ for all SOP8-packaged forms of the ZSC31014. See Table 3.7 for details.